Diminished arachidonate 5-lipoxygenase perturbs phase separation and transcriptional response of Runx2 to reverse pathological ventricular remodeling

Saiyang Xie,[a,b,e] Mengya Chen,[a,b,e] Wenxi Fang,[a,b,e] Shiqiang Liu,[a,b] Qingqing Wu,[a,b] Chen Liu,[a,b] Yun Xing,[a,b] Wenke Shi,[a,b] Man Xu,[a,b] Min Zhang,[a,b] Si Chen,[c] Xiaofeng Zeng,[c] Shasha Wang,[c] Wei Deng,[a,b,d,f,**] and Qizhu Tang[a,b,*,f]

[a]Department of Cardiology, Renmin Hospital of Wuhan University, Wuhan, China
[b]Hubei Key Laboratory of Metabolic and Chronic Diseases, Wuhan, China
[c]Cardiovascular Research Institute of Wuhan University, Wuhan 430060, China
[d]Department of Cardiology, The Fifth Affiliated Hospital of Xinjiang Medical University, Ürümqi, China

eBioMedicine
2022;86: 104359
Published Online XXX
https://doi.org/10.1016/j.ebiom.2022.104359

Summary

Background Arachidonate 5-lipoxygenase (Alox5) belongs to a class of nonheme iron-containing dioxygenases involved in the catalysis of leukotriene biosynthesis. However, the effects of Alox5 itself on pathological cardiac remodeling and heart failure remain elusive.

Methods The role of Alox5 in pathological cardiac remodeling was investigated by Alox5 genetic depletion, AAV9-mediated overexpression in cardiomyocytes, and a bone marrow (BM) transplantation approach. Neonatal rat cardiomyocytes were used to explore the effects of Alox5 in vitro. Molecular and signaling pathways were revealed by CUT &Tag, IP-MS, RNA sequencing and bioinformatic analyses.

Findings Untargeted metabolomics showed that serum 5-HETE (a primary product of Alox5) levels were little changed in patients with cardiac hypertrophy, while Alox5 expression was significantly upregulated in murine hypertensive cardiac samples and human cardiac samples of hypertrophy, which prompted us to test whether high Alox5 levels under hypertensive stimuli were directly associated with pathologic myocardium in an enzymatic activity-independent manner. Herein, we revealed that Alox5 deficiency significantly ameliorated transverse aortic constriction (TAC)-induced hypertrophy. Cardiomyocyte-specific Alox5 depletion attenuated hypertensive ventricular remodeling. Conversely, cardiac-specifical Alox5 overexpression showed a pro-hypertrophic cardiac phenotype. Ablation of Alox5 in bone marrow-derived cells did not affect pathological cardiac remodeling and heart failure. Mechanically, Runx2 was identified as a target of Alox5. In this regard, Alox5 PEST domain could directly bind to Runx2 PTS domain, promoting nuclear localization of Runx2 in an enzymatic activity-independent manner, simultaneously contributed to liquid–liquid phase separation (LLPS) of Runx2 at specific domain in the nucleus and increased transcription of EGFR in cardiomyocytes. Runx2 depletion alleviated hypertrophy in Ang II-pretreated Alox5-overexpressing cardiomyocytes.

Interpretation Overall, our study demonstrated that targeting Alox5 exerted a protective effect against cardiac remodeling and heart failure under hypertensive stimuli by disturbing LLPS of Runx2 and substantial reduction of EGFR transcription activation in cardiomyocytes. Our findings suggest that negative modulation of Alox5-Runx2 may provide a therapeutic approach against pathological cardiac remodeling and heart failure.

Funding National Natural Science Foundation of China.

Keywords: Arachidonate 5-lipoxygenase; Cardiac remodeling; Liquid–liquid phase separation; Runx2

*Corresponding author. Department of Cardiology, Renmin Hospital of Wuhan University, Jiefang Road 238, Wuhan 430060, China.
**Corresponding author. Department of Cardiology, Renmin Hospital of Wuhan University, Jiefang Road 238, Wuhan 430060, China.
E-mail addresses: qztang@whu.edu.cn (Q. Tang), vivideng1982@whu.edu.cn (W. Deng).
[e]These authors contributed equally.
[f]Co-corresponding authors.

Research in context

Evidence before this study

Alox5 is widely distributed in the human body and cells, and has attracted significant attention due to its ability to regulate immunity and inflammation in macrophages and neutrophils. Runx2 is a critical mechanistic link among mitosis, ribosomal biogenesis and cell fate, and is involved in cancer metastasis, vascular and valve calcification and neurodegenerative diseases. Liquid–liquid phase separation (LLPS) of transcription factors is essential for transcriptional activity and regulates multiple biological functions, including chromatin organization, mitophagy and nucleosome.

Added value of this study

High Alox5 levels under hypertensive stimuli were directly associated with cardiac hypertrophy in an enzymatic activity-independent manner. Genetic inhibition of Alox5 prevented chronic stress-induced pathological cardiac remodeling and heart failure. Loss of Alox5 disturbed the liquid–liquid phase separation of Runx2, which contributed to a substantial reduction of EGFR transcription in cardiomyocytes.

Implications of all the available evidence

Molecules that diminish Alox5 or disturbing the liquid–liquid phase separation of Runx2 may represent a therapeutic approach against pathologic ventricular remodeling and heart failure.

Introduction

Heart failure (HF) has long been considered a life-threatening disorder with high morbidity and mortality worldwide since it is the terminal stage of various cardiovascular diseases (CVDs). Importantly, cardiac remodeling, characterized by cardiac hypertrophy and fibrosis, has been established as a determining factor of the clinical course of HF.[1] Hypertrophy is regarded as an adaptive response in the short term. However, adverse remodeling develops under chronic stresses such as pressure overload,[2] ischemia,[3] neurohormonal alteration[4] and inflammation.[5] Suppressing pathological cardiac remodeling with technological and pharmaceutical interventions has become an appealing therapeutic strategy for HF. Notwithstanding that targeting Ca^{2+} channel,[6] β-adrenergic receptor[7] or the renin-angiotensin-aldosterone system (RAAS)[8] can protect against cardiac remodeling and improve the prognosis of HF patients, the overall efficacy of these agents remains limited. Accordingly, a deeper understanding of currently unknown risk factors for HF is necessary to facilitate the development of therapeutic strategies against HF.

As secondary signal transducers involved in multiple diseases, human lipoxygenases (LOXs) are enzymes that have been shown to participate in the metabolism of the polyunsaturated fatty acids and catalyze their oxidation to a variety of eicosanoids.[9] Multiple types of lipoxygenases have been documented in the literature, including Alox5, Alox12 and Alox15.[10] Alox12 deletion in mouse hearts or pharmacological inhibition can effectively attenuate ischemia-reperfusion cardiac injury.[11] Moreover, Alox15 inhibition can hinder inflammation and oxidative stress in the pathophysiology of diabetic cardiomyopathy.[12] Finally, Alox5 belongs to a class of LOXs involved as a potential therapeutic target against inflammation[13] and promotes 5-Oxo-6,8,11,14-eicosatetraenoic acid (5-oxo-ETE) production in patients with acute myocardial infarction (AMI).[14] An increasing body of evidence suggests that Alox5 is expressed in macrophages, monocytes, neutrophils and eosinophils.[15–17] Our previous study revealed the association between Alox5 and inflammatory storm,[18] and blockage of Alox5 was beneficial to patients with acute coronary syndrome (ACS).[19,20] However, little is currently known on the association of Alox5 with pathological cardiac remodeling, especially Alox5 expression in cardiomyocytes and its role in HF pathogenesis.

In a previous study, we reported that ablation of Alox5 markedly attenuated inflammatory storm in septic cardiomyopathy.[18] And Alox12 has been recently reported to improve ischemic cardiomyopathy in an enzymatic activity-independent manner.[11] However, it's not well-known whether Alox5 functions as signal transduction by itself in an enzymatic activity-independent manner. In the present study, 5-HETE (the primary product of Alox5) levels within serum and heart tissues were evaluated in patients with cardiac hypertrophy and mice subjected to TAC surgery by untargeted metabolomics, respectively. We explored the role of Alox5 in cardiac remodeling, and the expression and effects of Alox5 in patients with HF and rodents under TAC operation. The role of Alox5 in pathological cardiac remodeling was investigated by Alox5 genetic depletion, specific loss of Alox5 in cardiomyocytes, AAV9-mediated cardiac-specifical Alox5 overexpression and bone marrow transplantation. Molecular and signaling pathways were explored by CUT &Tag, IP-MS, RNA FISH, unbiased RNA sequencing and bioinformatic analyses. Importantly, our study contributed to understanding the role of Alox5 in cardiomyocytes and demonstrated its potential as a therapeutic target for treating pathological cardiac remodeling and heart failure.

Methods

Patient study

The analysis of human heart and peripheral blood samples was in accordance with the principles outlined in the Declaration of Helsinki and approved by the Renmin Hospital of Wuhan University Review Board. Informed consent was signed by all participants or their families. We enrolled 7 HF patients with left ventricular hypertrophy (LVH), 4 age- and sex-matched negative control subjects from Renmin Hospital of Wuhan University from July 2021 to December 2021 (Table S1). Structural parameters, including left ventricular internal dimension at end-diastole and end-systole (LVIDD and LVISD), interventricular septal thickness (IVST), and posterior wall thicknesses (PWTs), were evaluated by echocardiography. LVH was defined by the partition values of (left ventricular mass) LVM body surface area (BSA) above 125 g/m^2 for men and above 120 g/m^2 for women as previously described.[21] The LVM and BSA were calculated according to the following formula:

$$LVM\ (g) = 0.8 \times [1.04 \times (LVIDD + IVST + PWT)^3 - (LVID - (LVIDD)^3] + 0.6.$$

$$BSA\ (m^2) = 0.0061 \times height\ (cm) + 0.0125 \times weight\ (kg) - 0.1529.$$

Animals

All experimental animal procedures were in accordance with the National Institutes of Health (NIH) guidelines and were approved by the Animal Care and Use Committee of Renmin Hospital of Wuhan University (Approval No. WDRM20190211). Alox5 homozygous mutant mice (Alox5 KO, C57BL/6J background) were purchased from the Jackson Laboratory, the wild-type (WT) littermates as control. Myh6-$mcm^{+/-}$ Cre mice were purchased from the Jackson Laboratory (Cre was expressed under mouse cardiac-specific α-myosin heavy chain promoter (α-MHC; Myh6)); Alox5 fl/fl mice were obtained from Shanghai model organisms. Myh6-$mcm^{+/-}$ Cre mice were crossed with Alox5 fl/fl mice to generate Myh6-$mcm^{+/-}$cre; Alox5fl/fl mice. The Cre-mediated excision of floxed Alox5 alleles was induced by treatment with tamoxifen dissolved in corn oil by intraperitoneal injection at 20 mg kg^{-1} body weight per day for 5 consecutive days. C57BL/6J mice were purchased from the Institute of Laboratory Animal Science, Chinese Academy of Medical Sciences (Beijing, China) and housed in a quarantine room for at least a week, as previously described.[22] Eight to ten-week-old male mice were subjected to transverse aortic constriction (TAC) operation for 4 weeks to induce LV pressure overload. In the bone marrow (BM)-transplanted chimeric mice model, the BM cells were extracted from WT or Alox5 KO mice (CD45.2, C57 background) and tibias with PBS. After irradiation with two doses of 5.5 Gy at a 4-h interval,[23] recipient mice (CD45.1, SJL background) were injected with isolated BM, and mononuclear cells were analyzed for transplantation efficiency by flow cytometry 4 weeks later.[24] To induce exogenous expression of Alox5 gene in vivo, rAAV9-cTnT-Alox5 was utilized (Vi Gene Biosciences, China), More details were provided in Supplement Figure S10.

BM transplantation

Eight-week-old recipient mice (WT or Alox5 KO) were subjected to two irradiation doses of 5.5 Gy with a 4-h interval. BM cells from donor mice (WT or Alox5 KO) were collected in RPMI1640 medium. After irradiation, BM cells (>10^7) from donor mice were injected into recipient mice via caudal vein. 4 weeks after BM transplantation, mononuclear cells were analyzed for transplantation efficiency by flow cytometry and reconstituted mice were subjected to TAC surgery.

Echocardiography measurement

Echocardiography was performed following TAC for 4 weeks. As our previous study,[18] mice were anesthetized (2% isoflurane) and echocardiography was analyzed with a 10-MHz linear array ultrasound transducer equipped with a 30-MHz probe (Vevo 3100 system Visual Sonics). Some parameters were measured under the long-axis M-mode. Notably, the fractional shortening (FS) was calculated by the formula: LVFS = (LVIDd − LVIDs) × 100/LVIDd. The LV ejection fraction (LVEF) was also evaluated using the Teichholtz formula: LVEF = ([100 − Y] × 0.15) + Y; Y = (LVIDd2 − $LVIDs^2$) × 100/$LVIDd^2$.

Histological analysis

Heart tissues were fixed, embedded, and sectioned into 5 μm thick slices, as previously reported.[18] Sections were stained with Masson's trichrome for collagen volume analysis. Sections were stained with H&E or wheat germ agglutinin (WGA) to measure cardiac hypertrophy. For immunohistochemistry (IHC), prepared heart sections were incubated with antibodies against α-smooth muscle actin (α-SMA), CD68, Alox5 or BNP at 4 °C overnight, then with secondary antibodies at 37 °C for 1 h and detected with 3, 3′-diaminobenzidine, and sections were counterstained with hematoxylin. For immunofluorescence, frozen heart sections or cells were labeled with primary antibodies Alox5, Collagen I, α-actinin and Runx2, and then incubated with Alexa Fluor 568- or 488-oconjugated secondary antibody (Abcam). IHC, Masson's trichrome and H&E images were captured by Aperio VERSA 8 (Leica biosystems), while immunofluorescence and WGA images were captured by Olympus BX53. All images were analyzed by a person blinded to treatment by using Image J.

Isolation of cardiomyocytes

Adult mice were sacrificed before dissection of hearts, which were then washed with PBS to remove blood. Next, the heart was cut into pieces and fixed in ice cold fixation buffer (PBS containing 2% paraformaldehyde) for 2 h. Fixed heart fragments were washed in PBS and exposed to digestion buffer (PBS containing 1 mg/mL collagenase II) at 37 °C overnight. Cells were washed at the next day twice with PBS, counted with a hemocytometer and plated on SuperFrost Plus adhesion slides (Thermo scientific) for further processing.

Transcriptomic profiling and analysis

Total RNA was isolated from cardiac tissue of WT or Alox5 cKO mice treated or not with TAC surgery by TRIzol Reagent and RNeasy mini kits (QIAGEN). RNA quality was assessed with a 2100 Bioanalyzer, showing high RNA purity and integrity. RNA-seq libraries were prepared according to NEBNext Ultra II Directional RNA Library Prep Kit (New England Biolabs, Massachusetts, USA) and sequenced using an Illumina HiSeq 2500 System (single read 60bp). Library preparation and sequencing were performed by the CNIC's Genomics Unit. FastQ sequencing files were then processed and analyzed with the web tool RaNA-seq. Differentially expressed genes between groups were determined using moderated t-test with Limma and adjusted by Benjamini-Hochberg ($P < 0.1$). Gene set enrichment analysis was performed for KEGG. Only significant enrichments with a Benjamini Hochberg-adjusted P value of less than 0.01 were considered. For heatmaps, leading edge gene sets from selected enriched pathways were extracted, annotated with their respective TPM values, which were then converted into raw Z-scores and imported into GraphPad Prism 9.0 (GraphPad Software, USA) for heatmap generation.

Metabolite analysis by high-performance liquid chromatography (HPLC) and mass spectrometry (MS)

Cardiac biopsies from mice and plasma form patients were subjected to mass spectrometric metabolomics extract a maximum of information on a wide spectrum of metabolites. The standard and reagents included: acetonitrile, isopropanol, methanol, chloroform, acetic acid, formic acid, methoxyamine hydrochloride, MSTFA —N-methyl-N-(trimethylsilyl) trifluoroacetamide, pyridine, 3-nitrophenylhydrazine, N-(3-dimethylaminopropyl)-N′-ethylcarbodiimide hydrochloride (EDC), sulfosalicylic acid. All chemicals were purchased from Sigma–Aldrich unless otherwise noted.

To analyze metabolites, the samples were solubilized in tubes with ceramic beads using 1 ml of ice-cold lysate buffer (methanol/water, 9:1 v/v). Subsequently, the samples were homogenized three times for 20 s at 5500 rpm using a Precellys 24 tissue homogenizer (Bertin Technologies, Paris, France). The mixture was centrifuged at 15000 *g*, for 10 min at 4 °C to precipitate proteins and tissue residues. The upper phase of the supernatant (300 µl) was used for the UHPLC–MS, evaporated at 40 °C in a pneumatically assisted concentrator (Techne DB3). Dried extracts were then solubilized with 200 µl deionized/MilliQ water, aliquoted or transferred in LC vials and injected into UHPLC–MS or kept at –80 °C until injection.

RNA FISH assay

The Cy3-labeled EGFR RNA probe was designed and synthesized by Creative Bioarray to target EGFR mRNA. Briefly, the RNA probe targeting the end-to-head junction of EGFR as was labeled with Cy-3 in NRVMs. After fixing in a 4% paraformaldehyde solution, samples were rinsed in 1 × PBS, permeabilized in 1 × PBS with 0.5% Triton X-100 (10 min) and blocked in 3% BSA for 30 min at room temperature. Then NRVMs were transfected with Ad-GFP-Runx2 (supported by DesignGene Biotechnology (Shanghai, China)) overnight. Immediately after DAPI was added, images were taken with immunofluorescence confocal microscope (Leica, TCS SP8).

Immunoprecipitation-mass spectrometry (IP-MS)

Isolated cardiomyocytes from neonatal rats were washed with phosphate-buffered saline (PBS) and lysed with immunoprecipitation lysis buffer containing 100 µM phenylmethylsulfonyl fluoride (PMSF; Beyotime). The cell lysates were subjected to immunoprecipitation with 50 µl protein A-agarose and anti-Flag (1:50) antibody (Ab) or normal rabbit IgG (1 µg/ml). The candidate proteins interacting with Alox5 were identified by mass spectroscopy (supported by Wuhan GeneCreate Biological Engineering Co., Ltd.).

Chromatin immunoprecipitation (ChIP) assays

ChIP assays were carried out with EZ-ChIP kit (Millipore) according to manufacturer's protocol. Briefly, three biological replicates of cardiac fibroblast from NRVMs transfected with Ad-con or Ad-Runx2 for 48 h were treated with Ang II for 6 h. NRVMs were cross-linked with 1% paraformaldehyde, before lysis with cold PBS/protease inhibitor. Chromatin was sheared by 10 s of sonication (Covaris 220) interposed with 30 s pauses, repeated 10 times. Immunoprecipitation was performed overnight at 4 °C, via 4 µg of specific antibody or immunoglobulin G. Each IP sample was added to protein G agarose beads for 3 h incubation at 4 °C. The immunocomplexes were extracted and processed by reverse cross-linking, proteinase K digestion, and DNA precipitation. The following antibodies were used for Chip: rabbit anti-Runx2 antibody (Abcam, ab236639),

rabbit anti-acetyl-Histone H4 antibody (Millipore), and Ig G (Sigma). The following primers were used for EGFR Chip-PCR: forward 5′-CATTAAGGAGGCCT GTCTGCACCCGGAG-3′ and reverse 5′-GCACCCG-GAGTTGGGTGCCCTCATTTC-3′.

Luciferase reporter assays

The plasmid encoding luciferase reporter gene for EGFR was generated (pGL4.38[luc2P/EGFR RE/Hygro] Vector). The reporter plasmid was transfected into cells in 6-well plates with pcDNA3.1 encoding Runx2 as or blank pcDNA3.1 plasmid. 48 h later, HEK 293T cells were harvested and analyzed by a luminometer. Firefly activity was normalized to Renilla luciferase activity.

Cut&Tag assay

Cut&Tag assay was performed to identify the targeted molecule and sequence. Briefly, 10^5 cells were washed twice gently with wash buffer. 10 μL Concanavalin A coated magnetic beads were added per sample and incubated at RT for 10 min. Remove unbound supernatant and resuspended bead-bound cells with dig wash buffer and a 1:50 dilution of Runx2 primary antibody or IgG control antibody incubated overnight at 4 °C. The primary antibody was removed using magnet stand. Secondary antibody (Rabbit Anti-Mouse IgG H&L) was diluted 1:100 in dig wash buffer and cells were incubated at RT for 60 min Cells were washed using the magnet stand 2–3 times in dig wash buffer. A 1:100 dilution of pA-Tn5 adapter complex was prepared in digmed buffer and incubated with cells at RT for 1 h. Cells were washed in 1 mL Dig-med buffer. Then cells were resuspended in tag mentation buffer and incubated at 37 °C for 1 h. DNA was purified using phenol-chloroform-isoamyl alcohol extraction and ethanol precipitation. To amplify libraries, 21 μL DNA was mixed with 2 μL of a universal i5 and a uniquely barcoded i7 primer. A volume of 25 μL NEB Next HiFi 2 × PCR Master mix was added and mixed. The sample was placed in a Thermocycler with a heated lid using the indicated cycling conditions.

Plasmid constructs

The full-length Alox5, Runx2, Alox5(M) in H367N, H372N and H550N plasmids were obtained by cloning their cDNA into the Phage vector with corresponding HA, MBP or Flag tag. The DNA sequences of these constructs were verified by DNA sequencing.

Phase separation assays

Buffer containing 20 mM HEPES pH 7.5 and 200 mM NaCl, room temperature and 10 ml volume per system were used as general conditions for in vitro phase separation assays. Briefly, purified proteins were mixed with buffers containing 20 mM HEPES pH 7.5 and various concentrations of NaCl (0 and 1 M) at desired ratios to adjust the concentration of NaCl and proteins. For crowding agent induced LLPS, an additional buffer containing 20 mM HEPES pH 7.5, 200 mM NaCl and 50% PEG8000 (115, Merck) was added to adjust the final concentration of buffer constituents. For protease-induced LLPS, 0.5 ml of 5 mg/ml protease 3 °C were added into each system to initiate phase separation. All the proteins used in LLPS experiments were subjected to prior centrifugation to remove undissolved protein aggregates. After 2 min induction, each LLPS system was pipetted onto a glass slide and detected for DIC imaging. For sedimentation assays, LLPS was induced in the systems (volume 100 ml) for 5 min via cleavage of the MBP tag.

Fluorescence recovery after photobleaching (FRAP) assay

Ad-Runx2-GFP transfected NRVMs grown on glass coverslips were maintained in imaging buffer with Ang II-con-siRNA or Ang II-Alox5 siRNA. The FRAP measurement was performed in Leica TCS SP8 scanning confocal microscope with 60×/oil immersion objective, 488 nm Argon laser at 0.5% laser power during imaging and 1 iteration of 50% laser power during photobleaching (Leica).

For FRAP, a frame size of 512×512 pixels covering the whole nucleus was scanned at 4 frames/sec for 30 s post-bleach. A representative circular region of 2.9 μm diameter was bleached with one iteration (60 ms) of high intensity laser (50%). 25 pre-bleach images were taken and the last 10 pre-bleach fluorescence intensity values were averaged to normalize the post-bleach fluorescence recovery curve. We performed FRAP experiments on at least 20 cells per condition and repeated experiments at least twice. Individual FRAP measurement curves were averaged to get a single FRAP curve.

Adenovirus and siRNA transduction

NRVMs were infected with adenovirus encoding Alox5 (DesignGene Biotechnology, Shanghai, China) particles at MOI of 50 for 12 h, and Ad-LacZ was used as a control. Alox5 proteins were detected by immunoblot. Small siRNA oligos (RiboBio, Guangzhou, China) were transfected with Lipo-6000 reagent (Beyotime Biotechnology, China) following the manufacturer's instructions. Total RNA was extracted after 24 h to determine the effectiveness of siRNA transfection by immunoblot. The Alox5 silencing targeted sequence: 5′-GCATGACTTTGCTGACTTT-3′ and the control targeted sequence listed as 5′-GCTGCACA-GAGTTGCCTAA-3′. siRNAs targeting Runx2 (si-Runx2; 5′-CAGAAGAATGGTACAAATCCAAG-3′) and a negative control (NC) siRNA (si-NC; 5′-TTCTCCGAACGTGTC ACGTdTdT-3′) were constructed.

Total and nuclear proteins exaction, immunoblotting and co-immunoprecipitation

Isolated cardiomyocytes and myocardial tissue in indicated groups were lysed in radioimmunoprecipitation assay (RIPA) buffer (Servicebio, China). Nuclear protein extracts were isolated according to the introduction of commercial kits (Beyotime, P0027). In each group, 20 μg protein lysate was prepared for SDS-PAGE, and then the proteins were electrophoresed and transferred to PVDF membrane (Millipore, USA). After blocked for an hour, the primary antibody was incubated at 4 °C overnight. Next day, the chemical secondary antibody was incubated at room temperature for an hour, and the chemiluminescent protein detection developer (ECL, Broad, USA) was utilized with a chemiluminescence scanning membrane apparatus to obtain protein bands. Image J software was used to analysis Western blot strips. For immunoprecipitation, 20–30 mg myocardial tissue was cut into pieces, and then added with 1.0 mL IP lysate, and lysed for 30min at 4 °C, and collected lysate with 1 μg mouse IgG and 20 μl fully resuspended protein A + G Agarose (Beyotime Biotechnology, China), and shake slowly at 4 °C for 30min, then the lyse was centrifuged for 5 min in 2500 rpm and then collected the supernatant, and added with 1:800 dilution of the primary antibody to a 4 °C shaker overnight, and 40 μL of lyse was resuspended with Protein A + G Agarose in next day, and slowly shake at 1 °C for 1 h at 2500 rpm centrifuge for about 5 min, and carefully aspirated the supernatant, then washed the pellet 5 times with the lysate or PBS by preparing the protein sample. Then removed the supernatant, and added 20–40 μL of 1× SDS-PAGE electrophoresis loading buffer Vortex to resuspend the protein. When the protein was precipitated, the sample was centrifuged to the bottom of the tube by instantaneous high-speed centrifugation. After treated at 100 °C or boiling water bath for 3–5 min, some or all of the samples were taken for SDS-PAGE electrophoresis. The following antibodies were used: Alox5, α-Actinin, BNP, α-SMA, collagen I, Runx2, p-EGFR, EGFR, MED1, Lamin B1, β-Actin, p-P38, T-P38, p-ERK1/2, T-ERK1/2, p-JNK, T-JNK, DYKDDDDK and GST tag. More detail is provided in RRID Tag.

GST-pull down assay

The TNT coupled transcription and translation system (Promega) was used to transcribe and translate HA-Alox5 protein in vitro. Prokaryotically expressed GST-Runx2 in HEK 293T was purified with glutathione Sepharose 4B (GE Healthcare). HA-Alox5 protein and GST-Runx2 were co-incubated and rotated in 1% NP-40 buffer at 4 °C for 3 h. Subsequently, the protein complex was washed three times, eluted with 30 μl of 2 × SDS loading buffer and analyzed with Western Blotting assay.

RNA purification and qPCR

Total RNA was purified from tissue or cultured cell with Trizol (Invitrogen) following manufacturer's protocol. A part of total RNA was used for reverse transcription with SSTIII kit (Invitrogen) to generate cDNA. The cDNA is used in SYBR-based real-time qPCR on the following cycling conditions: hold for 2 min at 50 °C followed by 10 min at 95 °C to heat-start the Taq polymerase enzyme, then 40 cycles of 95 °C for 10 min, 60 °C for 1 min. Relative mRNA levels were analyzed using comparative Ct calculations normalized to β-Actin. The sequences of the primers for each gene detected are listed in Table S2.

Neonatal rat ventricular myocyte isolation and culture

Neonatal rat ventricular cardiomyocytes (NRVMs) were harvested from gender-free Sprague Dawley suckling rats within 3 days of birth, as previously described.[22] Under sterile conditions, the heart of the neonatal rat was isolated by thoracotomy and washed three times in precooling D-hank's buffer solution. Subsequently, the whole heart was cut into approximately 1.0 mm^3 particles. Afterward, the heart tissues were digested with 0.125% trypsin in a magnetic stirring apparatus at constant temperatures under 37 °C. NRVMs were purified from all collected cells by the differential adhesion method and cultured in 15% fetal bovine serum (FBS) within DEME/F12 medium at 37 °C in 5% CO_2. In addition, cell viability was detected by 0.4% trypan blue within an equal volume of cell suspension. Cardiomyocyte purity identification was performed after culture for 72 h. Briefly, Immunofluorescence (IF) targeting α-Actinin was performed. Ten high magnification fields were randomly selected to count the number of positive cells and the total number of cells. The purity of NRVMs was analyzed by positive cells/total number of cells ×100%.

Statistical analysis

All data presented in this study were presented as mean ± standard error of the mean (SEM). In the animal studies, we used $n \geq 6$ for biochemical analysis or pathology studies. In the cell culture studies, at least 3 independent replications was performed. Randomization and blinded conduct in all animal experiments. For all imaging analyses, an observer who was blind to the experimental groups conducted the quantitation. No samples or animals were excluded from the analysis. Student's t-test was applied for pairwise comparisons. For multiple group comparison, one-way or two-way ANOVA with Tukey post hoc test was performed. Differences were deemed statistically significant at $P < 0.05$. GraphPad Prism software (Version 9.0, GraphPad Software) and IBM SPSS Statistics 22.0 (IBM Corporation) were used for statistical analysis.

Role of funders
The Funders had no role in the study design, data collection, data analyses, interpretation, or writing of report, and the decision of paper submission.

Results

Alox5 is upregulated during pathological cardiac hypertrophy without change in its enzymatic activity

To investigate whether Alox5 signaling is associated with ventricular hypertrophy and heart failure, we assessed the Alox5 expression in heart tissues of patients diagnosed with heart failure. We found that Alox5, 5-lipoxygenase-activating protein (FLAP) and Myh7/β-MHC (β-myosin heavy chain) protein levels were significantly increased compared with normal hearts (Fig. 1a). In line with the data in immunoblot assays, a higher Alox5 and brain natriuretic peptide (BNP; a marker of HF) proteins were observed in the myocardium of patients with HF by immunohistochemistry (IHC) (Fig. 1b). Next, we evaluated the protein level of Alox5 signaling in murine cardiac hypertrophic model induced by transverse aortic constriction (TAC) (Figure S1a). Immunoblot assay showed that Alox5 and FLAP proteins were significantly upregulated after TAC surgery for 4 weeks (Fig. 1c), which were also verified by the data of immunofluorescence (IF) in the myocardium of mice (Fig. 1d and S1d). The transcription of Alox5 was also increased after TAC (Figure S1e). Subsequently, we investigated the changes of Alox5 in vitro hypertrophic model with neonatal rat ventricular cardiomyocytes (NRVMs) induced by angiotensin II (Ang II) treatment (Figure S1b). Interestingly, substantial production of Alox5 in time dependent manner was identified by immunoblot in NRVMs subjected to Ang II treatment (Figure S1c). Given the unique features of Alox5 distribution,[24,25] we performed further analyses on the subcellular localization of Alox5 in NRVMs. Immunoblot assay using isolated nuclear fraction or immunofluorescence was performed on NRVMs with or without Ang II treatment, by which we found that Ang II treatment contributed to Alox5 accumulation in the nucleus (Figs. 1e, f and S1f). To assess the enzymatic activity of Alox5 in patients with cardiac hypertrophy and HF, 5-HETE, the primary product of Alox5, was evaluated in the serum of patients with cardiac hypertrophy by untargeted metabolomics (Figure S1g, h). Both serum 5-HETE and 5-oxoETE levels were little changed in patients with or without cardiac hypertrophy (Fig. 1g). In addition, 5-HETE and 5-oxoETE were also detected in heart tissues of TAC-treated mice (Figure S1i, j). As expected, Serum 5-HETE and 5-oxoETE contents in TAC-treated mice were little changed from that in sham mice (Fig. 1h). Overall, these results suggest that upregulation of Alox5 was associated with cardiac hypertrophy without alteration in its enzymatic activity, implying that Alox5 expression in cardiomyocytes may play a critical role in controlling pathological cardiac remodeling and HF.

Ablation of Alox5 ameliorates pressure-overload induced cardiac remodeling and HF

We next evaluated the role of Alox5 in cardiac remodeling and HF by a loss-of-function approach (Fig. 2a and S2a–d), by which Alox5 knockout mice were subjected to TAC for 4 weeks to establish mouse HF model (Fig. 2a). Chronic stress induced a substantial increase in heart size, ratio of heart weight to body weight (HW/BW), ratio of heart weight to tibia length (HW/TL) and myocyte cross-sectional area, which were significantly reduced in Alox5 deficient mice (Fig. 2b–d). Moreover, knockout of Alox5 dramatically decreased mRNA levels of pro-hypertrophic markers in TAC-treated mice (Fig. 2e), and reduced proteins of ANP and β-MHC was observed in Alox5 deficient mice (Figure S2e, f). In addition, Alox5 KO mice exhibited reduced collagen deposition, with decreased α-smooth muscle actin (α-SMA) and collagen I production in the heart (Fig. 2f, g and S2e, f). Consistently, ablation of Alox5 downregulated mRNA levels of pro-fibrogenic markers in TAC-treated mice (Fig. 2e). Furthermore, we assess the effect of Alox5 upon inflammation in TAC-induced hearts and found that genetic depletion of Alox5 presented limited influence on inflammatory infiltrate in the heart after TAC surgery for 4 weeks (Figure S2g, h). Subsequently, the effects of Alox5 on cardiac structure and function were further assessed by echocardiography. Importantly, we uncovered that Alox5 deficiency alleviated TAC-induced systolic dysfunction, with increased LVEF and reduced LVIDs (Fig. 2h and i). These findings suggest that Alox5 deficiency exerts a protective effect against pathologic ventricular hypertrophy and fibrosis.

To investigate the effects of Alox5 deficiency on other cell types including microphages, endothelial cells and cardiac fibroblasts (cell types that can be linked to pathological ventricular remodeling in heart tissues). Interestingly, limited changes were observed in these cell types (Figure S3). Given that Alox5 was highly expressed in cardiomyocytes upon hypertrophic stimuli, we sought to determine the effects of Alox5 on cardiomyocytes by silencing Alox5 with small interfering RNA (siRNA) or adenovirus (Ad)-mediated Alox5 overexpression (Figure S4a, b, e, f). Analysis of the cross-sectional area of NRVMs showed that NRVMs incubated with Ang II exhibited an enlarged cell size, while Alox5 knockdown restored Ang II-induced cell hypertrophy (Figure S4c) and Alox5 overexpression aggravated monocytes hypertrophy (Figure S4g). Consistently, qPCR showed a significant decrease in hypertrophic molecules (Nppa and Nppb) in NRVMs

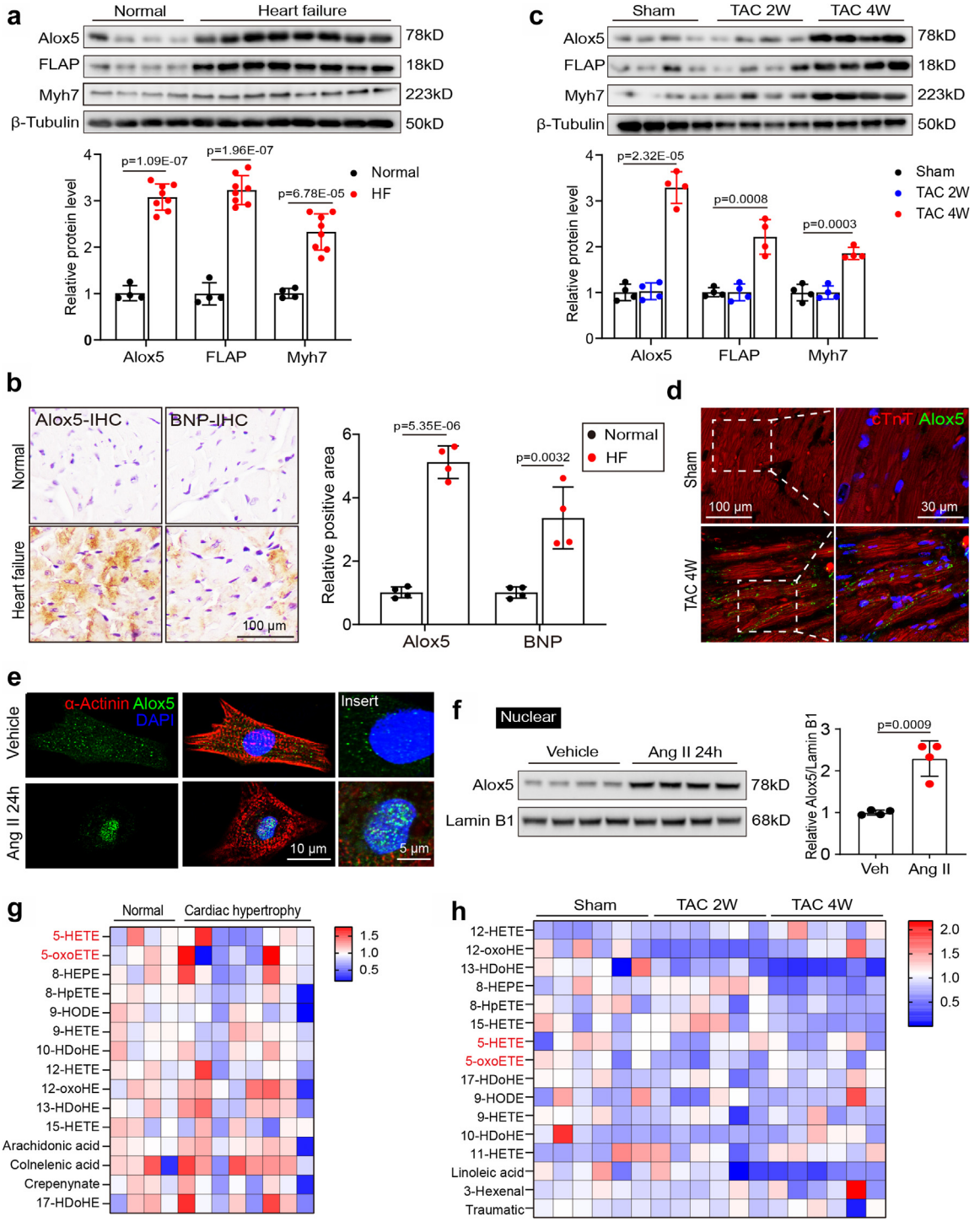

Fig. 1: **Identification of Alox5 as the crucial driving force in patients with HF, stress-induced isolated cardiomyocytes and cardiac remodeling mice. a.** Immunoblotting and quantitation of Alox5, 5-lipoxygenase-activating protein (FLAP) and MYH7/β-MHC (β-myosin heavy chain) protein levels in human heart tissue samples from normal donors (n = 4) and HF patients (n = 8). One-way ANOVA with Tukey's post-hoc test. **b.** Representative images of immunohistochemistry staining of Alox5 and brain natriuretic peptide (BNP) in human heart tissue samples from normal donors (n = 4) and HF patients (n = 4). One-way ANOVA with Tukey's post-hoc test. **c.** Immunoblot analysis of Alxo5, FLAP and Myh7 protein expression (upper) and quantification of the protein level normalized to β-Tubulin protein (lower) in C57BL/6J mice following sham or TAC for 2 and 4 weeks (n = 4). One-way ANOVA with Tukey's post-hoc test. **d.** Representative images of

subjected to Ang II and Alox5 siRNA (Figure S4d), suggesting that Alox5 knockdown alleviated myocyte hypertrophy in vitro under hypertrophic stimuli. By contrast, Alox5 overexpression led to substantially increased hypertrophic molecules (Nppa and Nppa) in NRVMs, implying Alox5 exacerbated Ang II-induced monocyte hypertrophy (Figure S4h). These results suggest that Alox5 controls cardiomyocyte growth under hypertrophic stimuli in vitro.

5-HETE enhanced macrophage-mediated inflammation induction, which could affect the outcome of a hypertrophic injury given the role of the macrophage in this setting. Herein, we sought to determine whether Alox5 derived from macrophages is involved in cardiac remodeling after TAC surgery by a BM transplantation approach (Figure S5a). Then, mice were bled 4 weeks after BM transplantation. Mononuclear cells were analyzed for transplantation efficiency by flow cytometry for CD45.1-APC and CD45.2-PE (Figure S5b), and suitable rodents were subjected to TAC for 4 weeks. Interestingly, mice carrying the Alox5 mutation exhibited reduced heart size compared to WT mice, while we observed no significant difference in Alox5 deficient mice who received WT BM or Alox5 KO BM transplantation (Figure S5c, d). Indeed, Alox5 depleted mice presented decreased myocyte cross-sectional area regardless of BM origin (Figure S5e). Similarly, Alox5-deficient mice displayed reduced transcription of hypertrophic genes (Nppa and Nppb) but no significant effects in mice that received either WT or Alox5 KO donor BM (Figure S5f). Moreover, BM transplantation yielded no effects on TAC-mediated cardiac fibrosis in Alox5 knockout mice, as demonstrated by immunofluorescence with collagen I, IHC and immunoblotting of α-SMA (Figure S5g, h), as well as qPCR of pro-fibrogenic genes (collagen I and Atac2) (Figure S5i). These results implied that Alox5 expression in BMDMs did not affect pathological cardiac remodeling following hypertrophic stimuli. We next explored the role of BMDMs-derived Alox5 on cardiac function after TAC surgery. A significant increase in systolic function was observed in Alox5 KO mice, whereas WT or Alox5 KO donor BM injection did not influence LVEF in TAC-treated Alox5 KO mice (Figure S5j, k). Conversely, using an inducible conditional deletion of Alox5 in cardiomyocytes (Alox5 conditional knockout (cKO)) (Fig. 3a; validation in Figure S6a, b), we found a substantial preservation of cardiac structure and function in Alox5 cKO mice after TAC surgery for 4 weeks. Notably, Alox5 cKO mice had a reduction of heart size, HW/BW, HW/TL and myocyte cross-sectional area compared with that in the Alox5 fl/fl mice (Fig. 3b–d). In addition, we found a lower ANP, BNP and β-MHC contents in Alox5 cKO mice after TAC surgery compared with littermate control mice (Fig. 3e and S6c, d). Similarly, pro-hypertrophic genes expression was dramatically downregulated at the level of transcription in Alox5 deficient hearts (Fig. 3f). On the other hand, Alox5 cKO mice exhibited reduced collagen deposition, with decreased α-smooth muscle actin (α-SMA) and collagen I production in TAC-treated hearts (Fig. 3g, h and S6c, d). Likewise, ablation of Alox5 in cardiomyocytes decreased mRNA levels of pro-fibrogenic markers in TAC-treated mice (Fig. 3i). Importantly, we found a substantial preservation of LVEF and improved systolic function in Alox5 cKO mice after TAC treatment, which was higher compared with littermate control mice (Fig. 3j and k). In addition, we investigated the effect of cardiomyocyte-specific Alox5 depletion upon heart inflammation in TAC-induced mice and uncovered that genetic depletion of Alox5 in cardiomyocytes presented limited influence on inflammatory infiltrate in the heart after TAC surgery for 4 weeks (Figure S6e, f). Collectively, these findings demonstrated that Alox5 expression in cardiomyocytes, not in bone marrow-derived macrophages, determined susceptibility to hypertrophic stimuli-induced ventricular remodeling and HF.

Loss of Alox5 counteracts MAPKs and EGFR signaling, and disrupts cytoplasmic-nuclear transport of Runx2 in an enzymatic activity-independent manner

To ascertain how Alox5 regulates cardiac remodeling under chronic hypertrophic stimuli, we evaluated transcriptomic alteration in adult mouse cardiomyocytes (AMCMs) from Alox5 fl/fl or Alox5 cKO mice (Fig. 4a). Accordingly, RNA sequencing (RNA-seq) and pathway analyses of differentially expressed genes (DEGs) in LV tissues showed a strong correlation between MAPKs and EGFR signaling pathways and Alox5 ablation in TAC-mediated hypertrophic AMCMs (Fig. 4b and c and Tables S3 and S4). Furthermore, by gene set enrichment analysis (GSEA) of RNA-seq data and direct immunoblotting analysis, we further validated that MAPKs and EGFR signaling were significantly reduced by Alox5

immunofluorescence staining of Alox5 (green) and cTnT (red) in C57BL/6J mice following sham or TAC for 4 weeks (n = 6). **e.** Representative images of immunofluorescence staining of Alox5 (Green) along with α-Actinin (Red) in NRVMs treated with vehicle or Ang II for 24h. **f.** Immunoblot analysis of Alxo5 protein expression (left) and quantification of the Alox5 protein level in nucleus normalized to Lamin B1 protein (right) in neonatal rat ventricular myocytes (NRVMs) treated with vehicle or angiotensin II (Ang II, 100 nM) for 24h (n = 4). Unpaired Student t-test. **g.** Heatmap generated by the one-to-one fold changes of identified metabolites in the arachidonic acid metabolism pathway in untargeted metabolomics dataset of human plasma samples. n = 4 for normal donors and n = 7 for HF patients with LV hypertrophy. **h.** Left ventricular contents of arachidonic acid pathway metabolites of mice at indicated time points during TAC surgery based on untargeted metabolomics (n = 6 mice for each group). All data are mean ± SEM. P values are indicated.

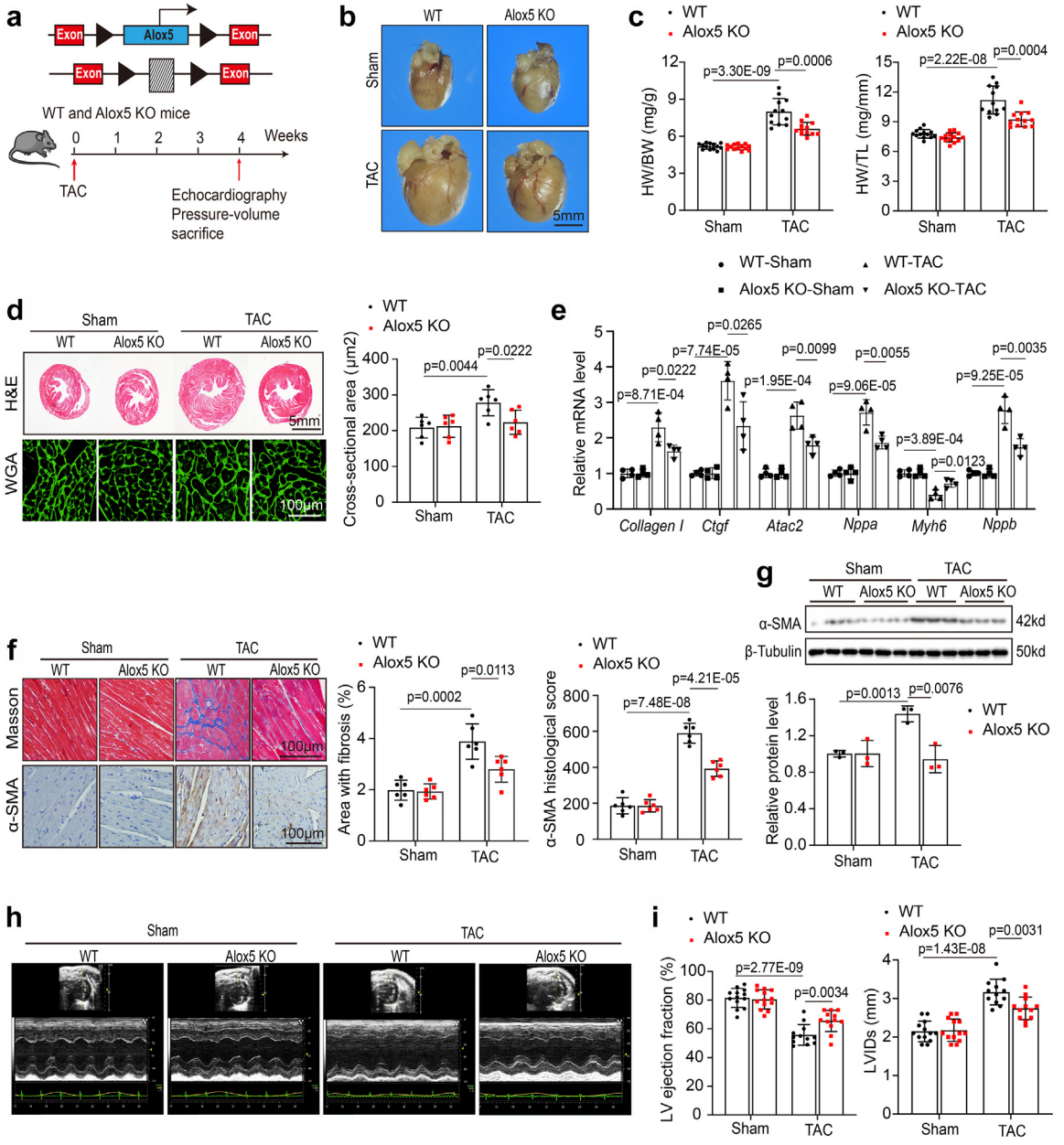

Fig. 2: **Genetic depletion of Alox5 attenuates cardiac hypertrophy, fibrosis and dysfunction in TAC-induced mice. a.** Schematic representation of Alox5 globally deficient mice generation (upper), and establishment of cardiac remodeling mouse model in WT or Alox5 mutant mice at 4 weeks after the TAC surgery (lower). **b.** Representative heart images in WT or Alox5 mutant mice at 4 weeks after the TAC surgery. **c.** Heart to body weight (HW/BW) and heart weight to tibia length (TL) ratios (n = 10–12). Two-way ANOVA with Tukey's post hoc test. **d.** Representative H&E and WGA-stained sections. Quantification of myocyte cross-sectional area (n = 6). Two-way ANOVA with Tukey's post hoc test. **e.** qPCR quantification of Collagen I, Ctgf, Atac2, Nppa, Myh6 and Nppb mRNA levels in LV of WT or Alox5 KO mice at 4 weeks after TAC (n = 4). Two-way ANOVA with Tukey's post hoc test. **f.** Representative cardiac Masson trichrome and IHC of α-SMA staining (left) and quantification of positive area with fibrosis (right) (n = 6). Two-way ANOVA with Tukey's post hoc test. **g.** α-SMA expression was evaluated by immunoblot and quantification normalized to β-Tubulin protein (n = 4). Two-way ANOVA with Tukey's post hoc test. **h.** Representative B- and M-mode echocardiographic imaging of heart. **i** and **j.** Analysis of LVEF and LVIDs of hearts subjected to TAC surgery (n = 11–13). Two-way ANOVA with Tukey's post hoc test. The results are shown as mean ± SEM. P values are indicated.

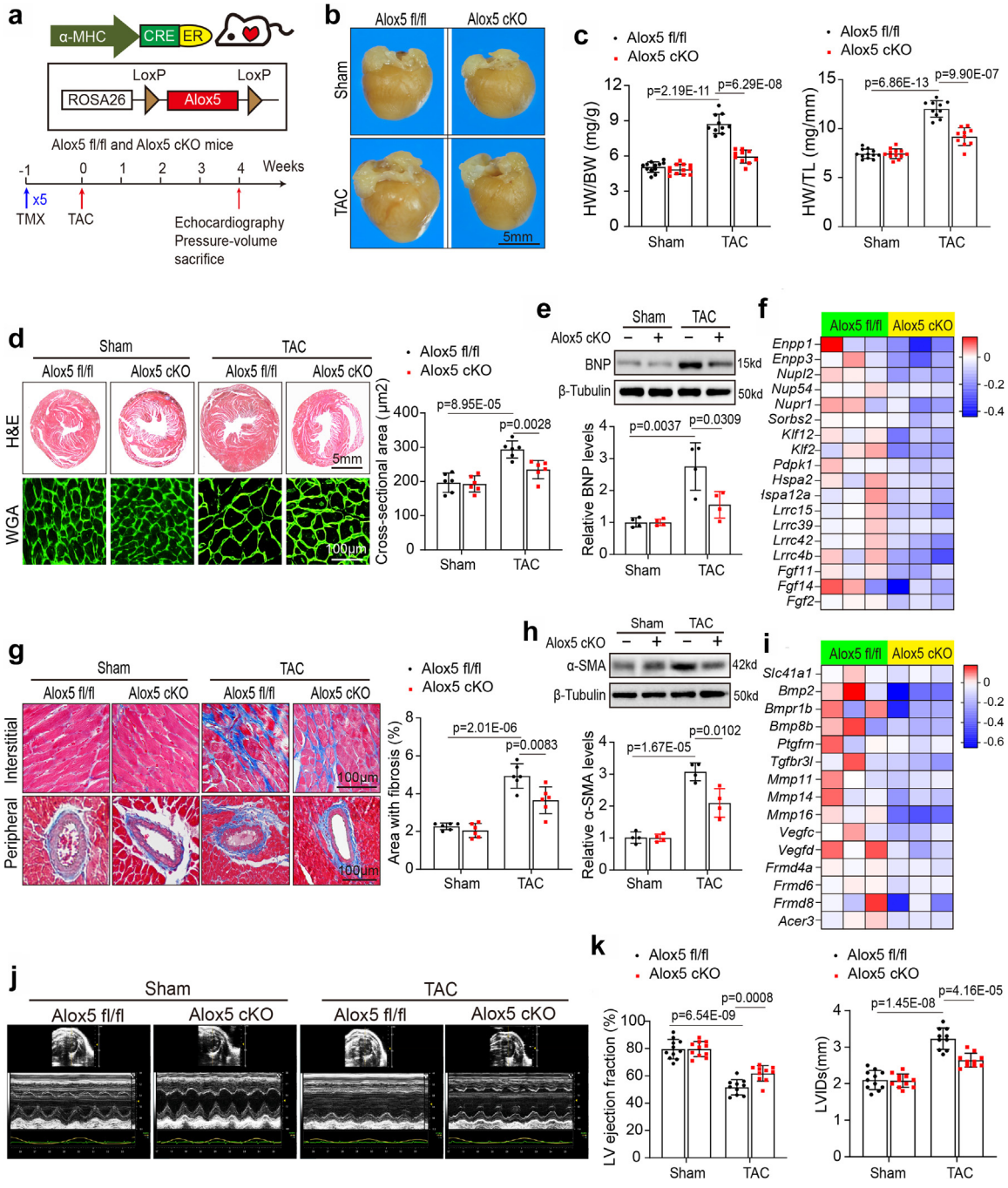

Fig. 3: **Cardiomyocyte-specific Alox5 ablation ameliorates cardiac remodeling and HF in TAC-induced mice. a.** Schematic representation of cardiac Alox5 specific deficient mice generation (upper), and establishment of cardiac remodeling mouse model in Alox5 fl/fl or Alox5 cKO mice at 4 weeks after the TAC surgery (lower). **b.** Representative heart images in Alox5 fl/fl or Alox5 cKO mice at 4 weeks after the TAC surgery. **c.** Heart to body weight (HW/BW) and heart weight to tibia length (TL) ratios (n = 10–12). Two-way ANOVA with Tukey's post hoc test. **d.** Representative H&E and WGA-stained sections. Quantification of myocyte cross-sectional area (n = 6). Two-way ANOVA with Tukey's post hoc test. **e.** BNP expression in LV was evaluated by immunoblot and quantification normalized to β-Tubulin protein (n = 4). Two-way ANOVA with Tukey's post hoc test. **f.** Heat map showing the hypertrophy-related genes expression in LV of Alox5 fl/fl or Alox5 cKO mice at 4 weeks after TAC (n = 3). **g.** Representative cardiac Masson trichrome staining in interstitial and peripheral area (left), and quantification of positive area with fibrosis (right) (n = 6). Two-way ANOVA with Tukey's post hoc test. **h.** α-SMA expression in LV was evaluated by immunoblot and quantification normalized to β-Tubulin protein (n = 4). Two-way ANOVA with Tukey's post hoc test. **i.** Heat map showing the pro-fibrogenic genes

deletion in isolated AMCMs (Fig. 4d–h). To further delineate the molecular basis for Alox5-mediated regulation of MAPKs and EGFR signaling, we further analyzed the mass-spectra dataset on the Alox5 immuno-precipitation (IP-MS) complex in NRVMs expressing the Flag-Alox5 protein by using Flag-GFP as a control (Figure S7a). 199 interacting proteins were uncovered by IP-MS (Fig. 5a and b and Table S5). Moreover, considering the enrichment of Alox5 in nucleus during hypertrophic stimuli (Fig. 1e and f), we focused on the protein candidates located in nucleus and detected enrichment of the proteins involved in transcription (Fig. 5d and e). Among these candidates, Runx2, a globally distributed transcription factor, rank as the top candidate for Alox5 binding in NRVMs (Fig. 5c). Immunoprecipitation (IP) analysis demonstrated an increased binding of Alox5/Runx2 in HF patient left ventricular (LV) tissues and AC16 human cardiomyocytes (Figure S7b, c). Similarly, Ang II treatment induced an enhanced interaction between Alox5 and Runx2 in NRVMs (Figure S7d). Alox5 preferentially bound to Runx2 in LV protein lysates of TAC-treated and Ang II infused mice relative to those of control mice (Figure S7e). *In vitro* protein binding assay also showed that GST-Runx2 and HA-Alox5 protein interacted (Fig. 5f). Consistently, immunofluorescence assays revealed that Alox5 was colocalized with Runx2 in the nucleus of NRVMs exposed to Ang II (Fig. 5g). Runx2 was closely bound to Alox5 in an Ang II-dependent manner in isolated cardiomyocytes (Fig. 5h). Given that Runx2 elicited biological functions through nuclear translocation,[26] we evaluated the potential causative role of Alox5 in Runx2 nuclear localization. Immunofluorescence analysis presented higher Runx2 contents in nuclear localization in heart tissues after TAC 4 weeks, which was dramatically reduced in Alox5 cKO mice (Fig. 5i). Interestingly, we also observed substantial Runx2 nuclear localization in NRVMs exposed to Ang II, while Alox5 silencing significantly abrogated nuclear translocation of Runx2 (Fig. 5j and S7f). To map the domain interaction between Alox5 and Runx2, we constructed several truncated mutants of Alox5, including Alox5ΔC2D, which lacks the first 118 amino acids of the N-terminus; Alox5ΔCD, in which the catalytic domain (CD) of Alox5 is deleted; and Alox5ΔPEST, which lacks C-terminal 155 amino acids of proline-, glutamic acid-, serine-, and threonine-rich motif. And we constructed several truncated mutants of Runx2, including Runx2ΔAD, which lacks AD1 and AD2 domain; Runx2ΔRunt, which lacks transcription domain Runt; Runx2ΔPTS, in which the AD3 and RD motifs are depleted; and Runx2ΔNLS, which lacks the C-terminal 61 amino acids of nuclear localization signal. By IP analysis, we demonstrated that Alox5 PEST domain bound to Runx2 PTS domain (Fig. 5k and l).

To assess the direct effect of 5-HETE (the primary product of Alox5) on Runx2 nuclear localization, we subsequently established an NRVM hypertrophic model with 5-HETE infusion. As expectedly, 5-HETE administration yielded a negligible impact on Runx2 distribution in NRVMs (Figure S8a, b), the opposite of the observations for Alox5 knockdown in NRVMs (Figs. 5j and S7f). Accordingly, we strongly hypothesized that the modulatory effect of Alox5 on myocytes was independent of enzymatic activity. To further delineate this issue, we designed an Alox5 enzyme-inactivation mutant Alox5(M) by substituting histidine residue with asparagine residue at positions 367, 372 or 550 (H367N, H372N and H550N),[27] which lacked enzymatic activity and suppressed 5-HETE production in the medium (Figure S8c). Interestingly, exogenous Alox5 supplementation markedly contributed to Runx2 nuclear localization following Ang II treatment. More importantly, Alox5(M) in H367N, H372N and H550N yielded a negligible impact on Runx2 distribution in cardiomyocytes (Figure S8d). These findings further suggest that depletion of Alox5 exerts a cardioprotective effect in cardiac remodeling and HF by disrupting the nuclear localization of Runx2 in an enzymatic activity-independent manner.

Depletion of Alox5 compromises transcription of EGFR through disruption of liquid–liquid phase separation (LLPS) of Runx2 in myocytes

Under normal growth conditions in NRVMs, the time-lapse record revealed the gradual formation of nuclear Runx2 puncta (Fig. 6a), consistent with the condensate formation observed in Ang II-treated NRVMs (Fig. 5j). Intriguingly, the endogenous nuclear Runx2 puncta in Ang II-treated myocytes was increased generation compare with untreated NRVMs and suppressed by Alox5 knockdown (Fig. 6a and S9b, c). Here, to further explore the bright and distinct punctate structures in the nucleus, we examined the amino-acid composition of human Runx2 using PONDR (http://www.pondr.com/). The Runx2 is highly enriched with low-complexity sequences (Figure S9a), suggesting that Runx2 may possess the capability to undergo LLPS. To explore this speculation, Ad-GFP-Runx2 was transfected with Ang II-treated NRVMs. Fluorescence recovery after photobleaching (FRAP) assays were performed and showed

expression in LV of Alox5 fl/fl or Alox5 cKO mice at 4 weeks after TAC (n = 3). **j** and **k.** Representative B- and M-mode echocardiographic imaging of heart **(j)**. Analysis of LVEF and LVIDs of hearts subjected to TAC surgery (n = 11–13) **(k)**. Two-way ANOVA with Tukey's post hoc test. The results are shown as mean ± SEM. P values are indicated.

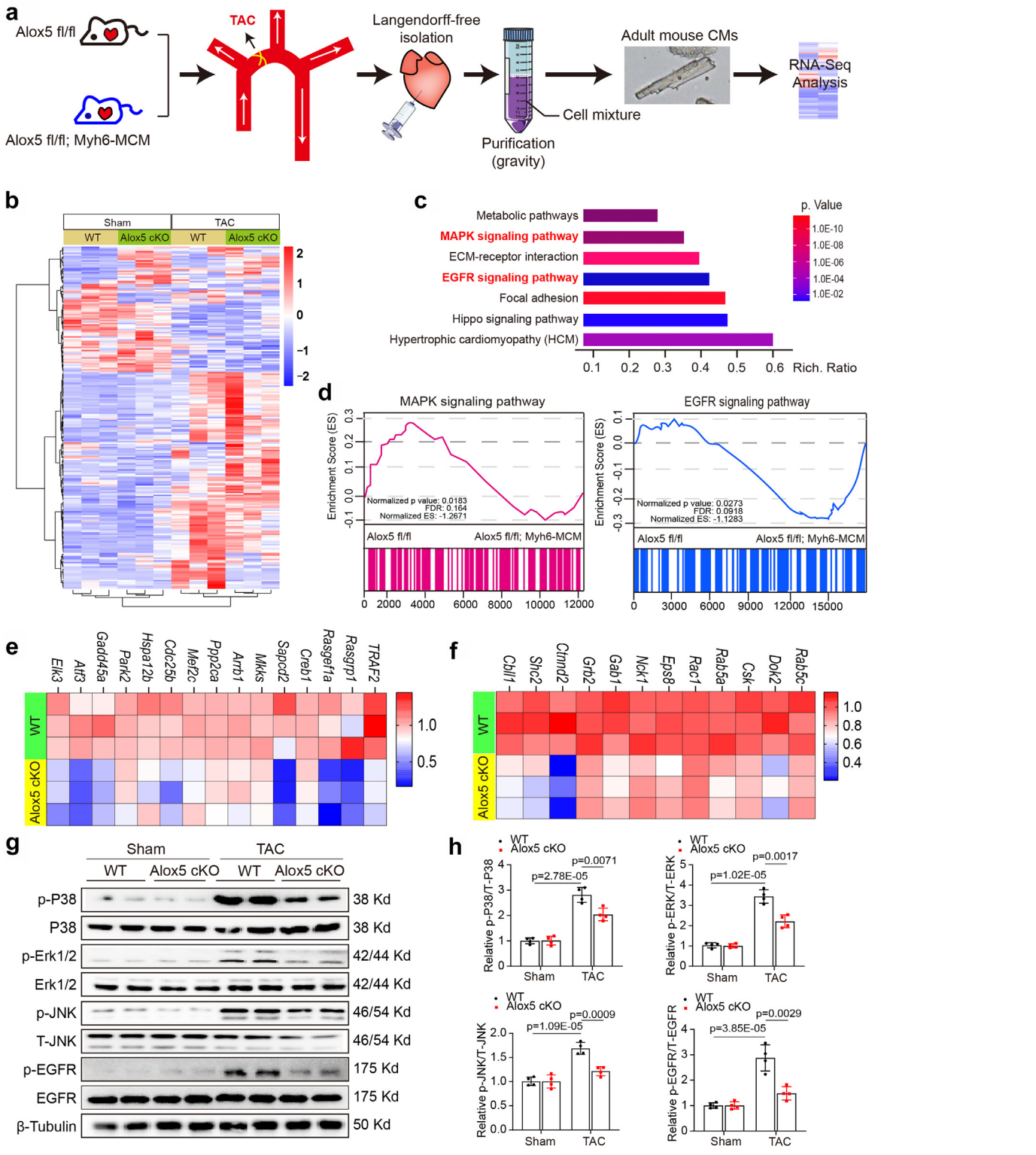

***Fig. 4:* Loss of Alox5 counteracts MAPKs and EGFR signaling. a.** Schematic diagram illustrating the experimental design to identify the key molecular events underlying Alox5 function in TAC-induced hypertrophy based on transcriptomics analysis. **b.** Heat map showing the general transcriptomic characteristics in Alox5 fl/fl and Alox5 cKO mice with sham or TAC surgery for 4 weeks (n = 3). **c.** Gene ontology (GO) analysis showing key molecular signatures both involved in cardiac remodeling process and regulated by Alox5. **d.** Gene Set Enrichment Analysis (GSEA)

that the fluorescence signal of GFP-Runx2 recovered to approximately 60% within 30 s after bleaching under Alox5 silencing, although the fluorescence signal recovered to 100% after bleaching under normal conditions (Fig. 6b and c and Videos S1 and S2). This finding suggests that GFP-Runx2 is highly mobile in the punctate structures in the nucleus and Alox5 siRNA co-incubation with NRVMs impeded the formation of Runx2 puncta. Given the universality of transcription,[28,29] the highly dynamic properties of Runx2 puncta in the nucleus prompted us to investigate whether Runx2 underwent liquid–liquid phase separation (LLPS) in myocytes. Subsequently, we analyzed the dynamic droplet by tagging Runx2 with maltose-binding protein (MBP) to achieve solubility-enhancement.[29] As expected, NRVMs with Ang II formed noticeable aggregated spherical droplets within 30 s, while markedly smaller puncta were observed under Alox5 silencing condition (Fig. 6d). This finding suggests that Alox5 triggers the liquid–liquid phase separation (LLPS) of Runx2 in myocytes.

We additionally investigated the target gene of Runx2 in cardiomyocytes by CUT & tag assay. Before Ang II treatment, NRVMs were transfected with either Runx2-overexpressing (Ad-Runx2) or empty (Ad-con) adenovirus. Subsequently, a CUT & tag assay and RNA-seq assay were performed following Runx2 overexpression verification (Figure S9d). 529 target genes were enriched by CUT & tag in Runx2-overexpressed cardiomyocytes (Figure S9e). And RNA-Seq analysis identified 653 upregulated DEGs in Runx2-overexpressed NRVMs. Here, 18 genes exhibiting significant mRNA alteration between WT and Runx2 overexpressing NRVMs were identified to directly bind with Runx2 (Figure S9f and Table S6). Among the target genes involved in EGFR and MAPK pathway, we focused on a significant Runx2-binding promoter region in the Egfr gene (Fig. 6e). Moreover, the ChIP assay confirmed significant enrichment of EGFR in Runx2-overexpressing NRVMs (Fig. 6f). The luciferase assay validated the interaction between Runx2 and the EGFR promoter (Figure S9g). In the meantime, the transcriptional mediator complex, which includes the subunit MED1, forms punctate structures in the nucleus,[30] and we found that Runx2 puncta partially co-localized with MED1 puncta, however, Alox5 knockdown greatly suppressed $Runx2^{+}$ $MED1^{+}$ puncta in the nucleus (Figure S9h, i). To examine the relationship between Runx2 puncta and EGFR mRNA under hypertrophic stimuli, we performed independent RNA-FISH experiments with Ad-GFP-Runx2 and EGFR mRNA probe co-incubation in NRVMs. Importantly, Runx2 punctate structures were colocalized with EGFR mRNA in the nucleus and significantly suppressed by Alox5 deletion (Fig. 6g and h). These findings suggested that Runx2 could target the EGFR promoter and regulate EGFR expression in cardiomyocytes.

Overall, our findings suggest that Alox5 mutation compromises transcription of EGFR through disruption of the liquid–liquid phase separation (LLPS) of Runx2 in cardiomyocytes.

Knockdown of Runx2 abrogates Alox5 overexpression-mediated cardiomyocyte hypertrophy *in vitro*

To identify which protein domains of Runx2 are responsible for LLPS, we generated five deletions mutants of Runx2 with deletions of the transcriptional activation domain 1 (AD1), transcriptional activation domain 2 (AD2), Runt domain, transcriptional activation domain 3 (AD3) and transcriptional repression domain (RD)—Runx2ΔAD1, Runx2ΔAD2, Runx2ΔRunt, Runx2ΔAD3 and Runx2ΔRD, respectively—and detected their distribution in Ang II-treated cells (Fig. 7a). Interestingly, Runx2ΔRD demonstrated substantially suppressed LLPS compared with full-length Runx2 and other deletion mutants (Fig. 7b). Consistent with the in vitro observation in protein binding assay, Alox5 PEST domain bound to Runx2 PTS domain (including RD domain) (Fig. 5k and l), indicating the importance of the RD domain for Runx2 LLPS and interaction with Alox5.

To explore whether Alox5 triggers hypertrophy and enhanced expression of EGFR and MAPK pathways in isolated cardiomyocytes by targeting Runx2. We induced Ang II-mediated hypertrophy of NRVMs that were incubated with or without Ad-Alox5 along with Runx2 siRNA or control siRNA. Alox5 overexpression resulted in enlarged cardiomyocyte size and enhanced mRNA expression of Nppa following Ang II treatment. However, these effects were disrupted by Runx2 silencing (Fig. 7c and d). Furthermore, Ad-Alox5 transfection significantly activated EGFR, P38, JNK and ERK1/2 signaling in Ang II-treated NRVMs, while Runx2 silencing conversely counteracted EGFR and MAPK pathway activation (Fig. 7e and f), indicating that targeting Runx2 in cardiomyocytes

showing the enrichment score of MAPK and EGFR signaling pathway gene sets in the heart tissue of Alox5 cKO and Alox5 fl/fl mice after TAC surgery for 4 weeks. **e** and **f.** Heat map showing the expression profile of MAPK and EGFR signaling pathway gene sets in the heart tissue of Alox5 cKO and Alox5 fl/fl mice after TAC surgery for 4 weeks. **g** and **h.** Immunoblotting and quantitation of phosphorylated and total expression of P38, ERK1/2, JNK and EGFR in the heart tissue of Alox5 cKO and Alox5 fl/fl mice after sham or TAC surgery for 4 weeks. Two-way ANOVA with Tukey's post hoc test. The results are shown as mean ± SEM. P values are indicated.

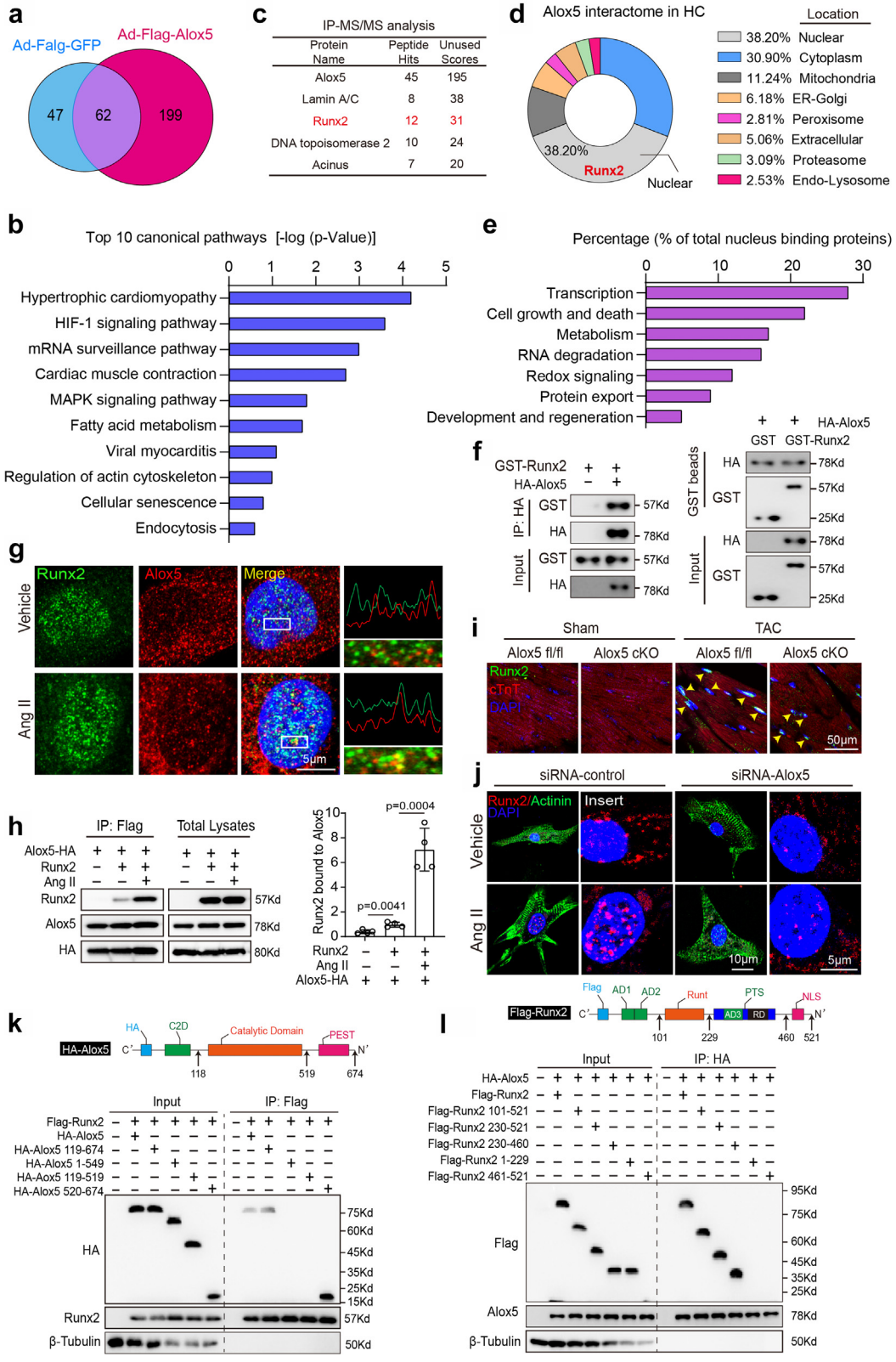
a
Ad-Falg-GFP
Ad-Flag-Alox5
47
62
199
c
IP-MS/MS analysis
Protein Name | Peptide Hits | Unused Scores
Alox5 | 45 | 195
Lamin A/C | 8 | 38
Runx2 | 12 | 31
DNA topoisomerase 2 | 10 | 24
Acinus | 7 | 20
d
Alox5 interactome in HC
Location
38.20% Nuclear
30.90% Cytoplasm
11.24% Mitochondria
6.18% ER-Golgi
2.81% Peroxisome
5.06% Extracellular
3.09% Proteasome
2.53% Endo-Lysosome
38.20%
Runx2
Nuclear
b
Top 10 canonical pathways [-log (p-Value)]
Hypertrophic cardiomyopathy
HIF-1 signaling pathway
mRNA surveillance pathway
Cardiac muscle contraction
MAPK signaling pathway
Fatty acid metabolism
Viral myocarditis
Regulation of actin cytoskeleton
Cellular senescence
Endocytosis
e
Percentage (% of total nucleus binding proteins)
Transcription
Cell growth and death
Metabolism
RNA degradation
Redox signaling
Protein export
Development and regeneration
f
GST-Runx2
HA-Alox5
IP: HA
GST beads
Input
GST
HA
57Kd
78Kd
25Kd
g
Runx2
Alox5
Merge
Vehicle
Ang II
5μm
h
IP: Flag
Total Lysates
Alox5-HA
Runx2
Ang II
Alox5
HA
80Kd
p=0.0004
p=0.0041
Runx2 bound to Alox5
i
Sham
TAC
Alox5 fl/fl
Alox5 cKO
Runx2
cTnT
DAPI
50μm
j
siRNA-control
siRNA-Alox5
Runx2/Actinin
DAPI
Insert
10μm
5μm
k
HA-Alox5
HA
C2D
Catalytic Domain
PEST
118
519
674
Flag-Runx2
HA-Alox5 119-674
HA-Alox5 1-549
HA-Aox5 119-519
HA-Alox5 520-674
75Kd
60Kd
45Kd
35Kd
25Kd
15Kd
β-Tubulin
50Kd
l
Flag-Runx2
Flag
AD1
AD2
Runt
PTS
NLS
AD3
RD
101
229
460
521
Flag-Runx2 101-521
Flag-Runx2 230-521
Flag-Runx2 230-460
Flag-Runx2 1-229
Flag-Runx2 461-521
95Kd

abrogates Alox5 overexpression-mediated adverse effect in cell hypertrophy.

Taken together, these results showed that the RD domain was required for Runx2 LLPS and interaction with Alox5, and Runx2 depletion reserves Alox5-induced adverse effect in hypertrophy.

Alox5 overexpression in cardiomyocytes exaggerates ventricular remodeling

To provide compelling evidence that upregulation of Alox5 in myocytes is closely associated with hypertensive ventricular remodeling and HF, a recombinant AAV9-cTnT mediated Alox5 overexpression mouse model was established (Figure S10a). To investigate the role of exogenous Alox5 in ventricular remodeling and HF, Alox5 overexpressing rodents were subjected to TAC operation for 4 weeks (Figure S10b), and the efficiency of AAV9 transfection was assessed by immunoblot in heart tissues (Figure S10c, d). As expected, overexpression of Alox5 in myocyte further exacerbated TAC-induced reduction in LVEF and increase in LVIDs (Fig. 8a and b). In addition, rodents treated with AAV9-Alox5 injection exhibited a larger cardiac size following TAC operation, with increased HW/BW, HW/TL and myocyte cross-sectional area (Fig. 8c–e). Moreover, Masson trichrome staining showed that exogenous Alox5 administration resulted in more cardiac collagen deposition in TAC-treated mice (Fig. 8f). Consistently, qPCR showed that Alox5 overexpression further promoted the transcription of pro-fibrogenic genes including collagen I, α-SMA and TGFβ in cardiac tissues (Fig. 8g). Also, data of immunoblot presented that Alox5 overexpression promoted Runx2-EFGR signaling after TAC (Fig. 8h and i). Overall, these data suggested Alox5 overexpression in cardiomyocyte accelerated TAC-induced ventricular remodeling.

Discussion

Although multiple interventions, including pharmacotherapy,[31] gene therapy[32] and mRNA-based CAR-T cell therapy,[33] have recently been shown to be beneficial against cardiac remodeling and HF, the occurrence of cardiac remodeling and HF has steadily increased. In the current study, we observed serum 5-HETE and 5-oxoETE were little changed in patients with cardiac hypertrophy, while Alox5 expression was significantly upregulated in murine hypertensive cardiac samples and human cardiac samples of hypertrophy. More importantly, we underlined that Alox5 expression in cardiomyocytes, not in bone marrow-derived macrophages, could determine susceptibility to cardiac remodeling and HF. Also, cardiac-specifical Alox5 overexpression exaggerates TAC-induced cardiac remodeling. Besides, we demonstrated that Alox5 could directly bind to Runx2 and promote nuclear localization of Runx2 in an enzymatic activity-independent manner, which contributed to liquid–liquid phase separation (LLPS) of Runx2 in the nucleus, promoting activation of EGFR and MAPKs pathways in cardiomyocytes. Moreover, the LLPS of Runx2 was identified as a regulated form of ventricular remodeling in current study, by which LLPS of transcription factor maybe a potential extension for CVDs. Herein, we identified Alox5 as the critical driving force behind cardiac remodeling and HF and hypothesized that Alox5 could be a potential therapeutic target for cardiac structure remodeling and dysfunction.

Alox5 has long been recognized as a lipoxygenase that can catalyze polyunsaturated fatty acids (e.g., arachidonic acid) transformation to inflammatory mediators,[34] and is reportedly involved in multiple pathophysiological functions, including cancer,[35] kidney damage,[35] obesity,[36] liver fibrosis[37] and atherosclerosis.[38] However, the underlying function of Alox5 on pathological cardiac remodeling and HF is unknown, nor is it

Fig. 5: **Alox5 directly binds to Runx2 and triggers cytoplasmic-nuclear transport of Runx2. a.** An overlap was performed between pull-down proteins in Ad-Flag-GFP- and Ad-Flag-Alox5-incubated NRVMs lysates. **b.** The molecular and cellular functions of the 199 Alox5 interactors in Ad-Flag-Alox5-incubated NRVMs are shown. **c.** Mass spectrometry analysis of Alox5 immuno-precipitates. Selected peptide hits and unused score are shown. Higher unused score means more credible. **d** and **e.** Cellular location of the Alox5 interactors in Ad-Flag-Alox5-incubated NRVMs. In particular, 32% of proteins are located in the nucleus. Runx2 ranked as a top candidate. Among nuclear candidates, transcription and cell growth and death are enriched. **f.** GST-Runx2 and Alox5-HA purified proteins were incubated in vitro for 30 min. Left: IP with anti-HA antibodies followed by Western blot with the indicated antibodies. Right: GST pull down analysis. **g.** NRVMs subjected to Ang II or vehicle. Representative images of immunofluorescence staining of Runx2 (Green) along with Alox5 (Red) in NRVMs (left), and analyses of co-location curve (right). **h.** Representative immunoblot (left) and relative quantification (right) of Alox5 bound to Runx2 in NRVMs transfected with Ad-Alox5-HA and/or Ad-Runx2 and treated with Ang II (n = 4). **i.** Representative images of immunofluorescence staining of Runx2 (Green) along with α-Actinin (Red) in heart tissues (n = 6). Arrow indicated Runx2-positive nuclear. **j.** NRVMs transfected with Alox5 or control siRNA were subjected to Ang II or vehicle. Representative images of immunofluorescence staining of Runx2 (Red) in nuclear. **k.** Flag-Runx2, full-length HA-Alox5, or truncated mutants of Alox5 were co-expressed in 293T cells for co-IP assay with anti-HA antibody. C2D, Ca^{2+} binding domain; PEST, proline-, glutamic acid-, serine-, and threonine-rich motif. **l.** HA-Alox5, full-length Flag-Runx2, or truncated mutants of Runx2 were co-expressed in 293T cells for co-IP assay with anti-Flag antibody. AD1, transcriptional activation domain 1; AD2, transcriptional activation domain 2; AD3, transcriptional activation domain 3; RD, transcriptional repression domain; PTS, proline-, serine-, and threonine-rich motif; NLS, nuclear localization signal.

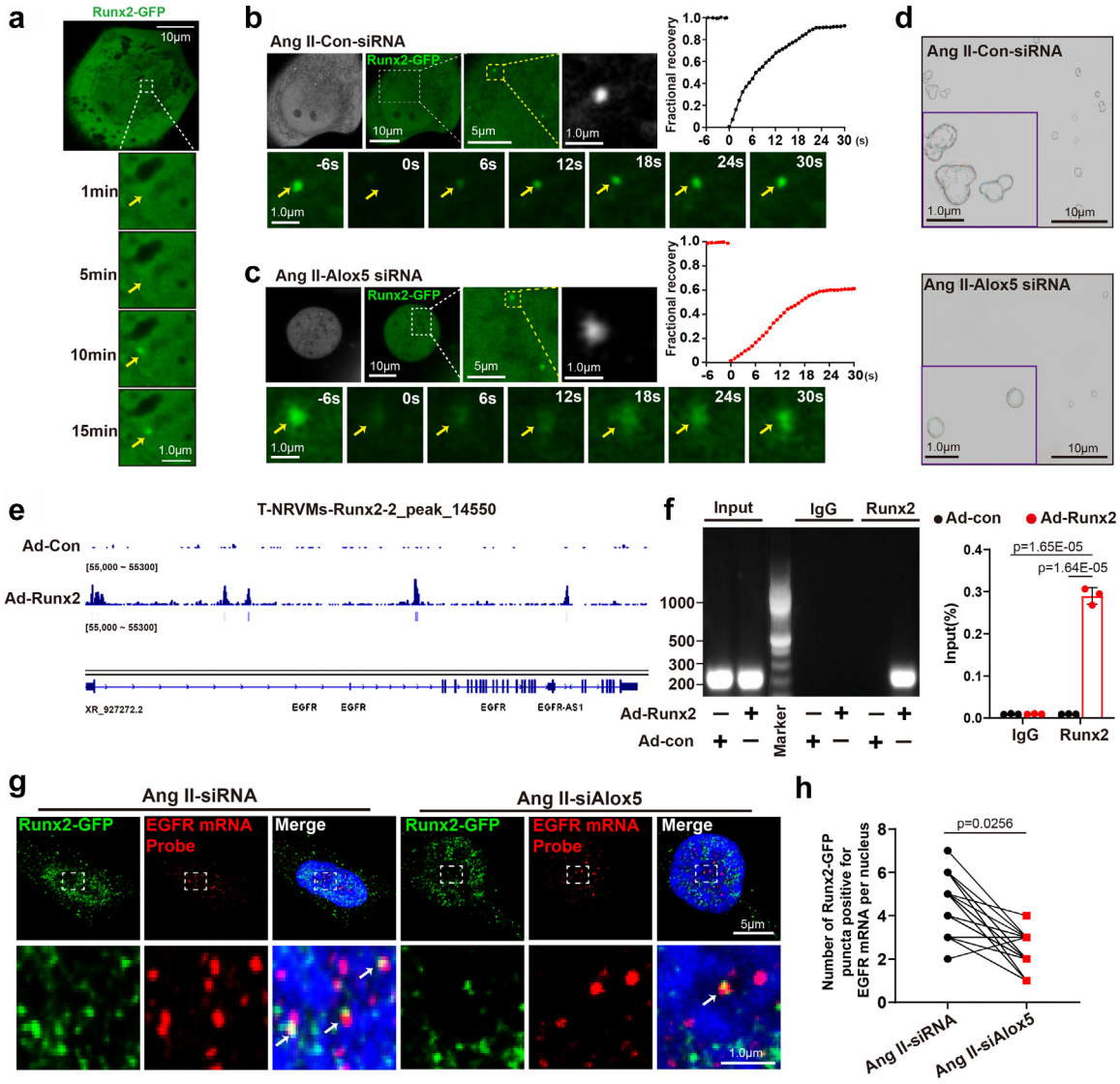

Fig. 6: **Alox5 mutation compromises transcription of EGFR through disruption of liquid–liquid phase separation (LLPS) of Runx2 in cardiomyocytes. a.** Time-lapse analysis of the formation of Runx2-GFP puncta upon Ang II in NRVMs transfected with Ad-Runx2-GFP. **b** and **c.** FRAP analysis of the Runx2-GFP signal of the punctate structures in the nucleus in NRVMs transfected with Runx2-GFP after Ang II-control-siRNA (**b**) or Ang II-Alox5-siRNA (**c**). And the quantification of fluorescence recovery after photobleaching (FRAP) by representing the fractional recovery, which refers to the fraction of the difference between the intensity before and immediately after bleaching. **d.** LLPS of Runx2 in a buffer containing NaCl, as shown by DIC imaging. DIC, differential interference contrast. **e.** Cut & tag map of the EGFR locus revealing Runx2 binding in NRVMs infected with Ad-con or Ad-Runx2. **f.** The independent ChIP assay was performed on Ad-con- or Ad-Runx2 infected NRVMs to verify Runx2 binding to the promoter regions of the EGFR gene. Two-way ANOVA with Tukey's post hoc test. **g** and **h.** In RNA-FISH assays, Runx2-GFP puncta colocalize with EGFR mRNA in NRVMs under Ang II-siRNA or Ang II-Alox5 siRNA treatment transfected with Runx2-GFP and quantification of double positive foci. Unpaired Student t-test. The results are shown as mean ± SEM. P values are indicated.

clear whether Alox5 function is independent of lipoxygenase activity. Our study sought to fill this research gap and demonstrated that Alox5 interacted with Runx2 and contributed to Runx2 nuclear localization in an enzyme-independent manner, providing a viewpoint that Alox5 exhibits an enzyme independent activity under hypertrophic stimuli in cardiomyocytes. It has been established that 5-HETE is the primary product in Alox5-mediated reactions[39] and 5-HETE is closely associated with AMI and septic cardiomyopathy. We conversely found that both 5-HETE and 5-oxoETE levels were little changed in mice and patients with cardiac hypertrophy, showing that the lipoxygenase activity of Alox5 was rarely associated with ventricular hypertrophy

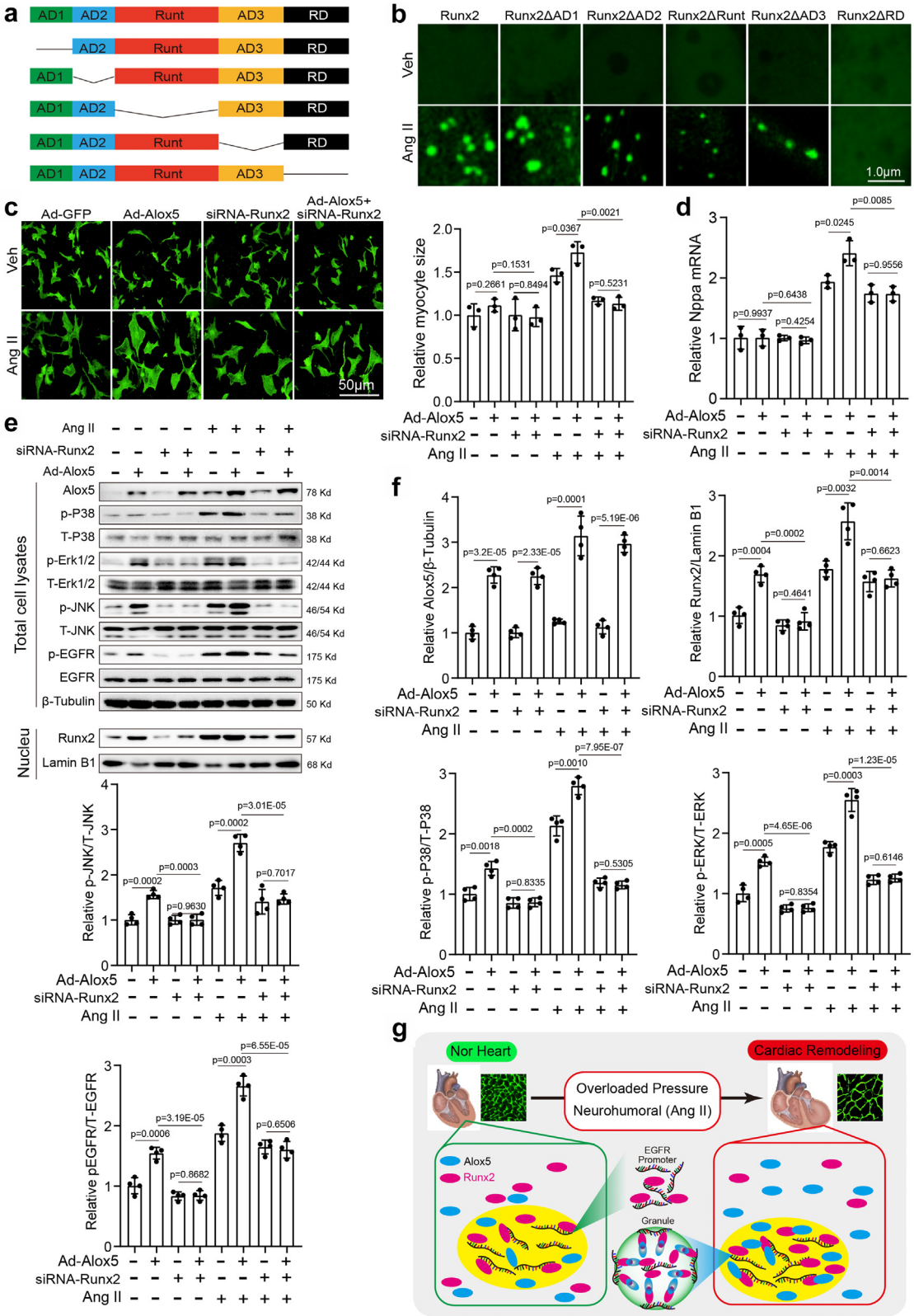
a
AD1 AD2 Runt AD3 RD
AD2 Runt AD3 RD
AD1 Runt AD3 RD
AD1 AD2 AD3 RD
AD1 AD2 Runt RD
AD1 AD2 Runt AD3
b
Runx2
Runx2ΔAD1
Runx2ΔAD2
Runx2ΔRunt
Runx2ΔAD3
Runx2ΔRD
Veh
Ang II
1.0μm
c
Ad-GFP
Ad-Alox5
siRNA-Runx2
Ad-Alox5+ siRNA-Runx2
Veh
Ang II
50μm
Relative myocyte size
p=0.2661 p=0.8494 p=0.1531 p=0.0367 p=0.0021 p=0.5231
d
Relative Nppa mRNA
p=0.9937 p=0.4254 p=0.6438 p=0.0245 p=0.0085 p=0.9556
Ad-Alox5
siRNA-Runx2
Ang II
e
Ang II
siRNA-Runx2
Ad-Alox5
Total cell lysates
Alox5 78 Kd
p-P38 38 Kd
T-P38 38 Kd
p-Erk1/2 42/44 Kd
T-Erk1/2 42/44 Kd
p-JNK 46/54 Kd
T-JNK 46/54 Kd
p-EGFR 175 Kd
EGFR 175 Kd
β-Tubulin 50 Kd
Nucleu
Runx2 57 Kd
Lamin B1 68 Kd
Relative p-JNK/T-JNK
p=0.0002 p=0.0003 p=0.9630 p=0.0002 p=3.01E-05 p=0.7017
Relative pEGFR/T-EGFR
p=0.0006 p=3.19E-05 p=0.8682 p=0.0003 p=6.55E-05 p=0.6506
f
Relative Alox5/β-Tubulin
p=3.2E-05 p=2.33E-05 p=0.0001 p=5.19E-06
Relative Runx2/Lamin B1
p=0.0004 p=0.0002 p=0.4641 p=0.0032 p=0.0014 p=0.6623
Relative p-P38/T-P38
p=0.0018 p=0.0002 p=0.8335 p=0.0010 p=7.95E-07 p=0.5305
Relative p-ERK/T-ERK
p=0.0005 p=4.65E-06 p=0.8354 p=0.0003 p=1.23E-05 p=0.6146
g
Nor Heart
Cardiac Remodeling
Overloaded Pressure
Neurohumoral (Ang II)
Alox5
Runx2
EGFR Promoter
Granule

following chronic pressure stress. As an important lipoxygenase, Alox5 is widely distributed in the human body and cells.[40] In recent years, Alox5 has attracted significant attention due to its ability to regulate immunity and inflammation in macrophages and neutrophils.[41] In contrast, the role of Alox5 signaling in parenchyma cells has been largely understudied. To the best of our knowledge, this study underlines that Alox5 expression in cardiomyocytes, not in bone marrow-derived macrophages, could determine susceptibility to hypertrophic stimuli-induced ventricular remodeling and HF. Also, both endothelial cells and cardiac fibroblasts are connected with pathological ventricular remodeling, although alox5 expression displays no alteration in response to hypertrophic stimuli. Therefore, the effects of Alox5 deficiency on other cell types need to be more research. Besides, previous studies have shown the unique features of interval Alox5 distribution.[24,25] Herein, we further performed analyses on the subcellular localization of Alox5 in NRVMs and uncovered that Alox5 expression was slightly increased in the cytoplasm and markedly upregulated in the nucleus during hypertrophic stress. We previously revealed the association between Alox5 expression and cardiac inflammatory storm,[18] and blockage of Alox5 was beneficial for patients with acute coronary syndrome (ACS).[19,42] However, this study revealed Alox5 impeded pathological ventricular remodeling and HF independent on its enzymatic activity.

Mammalian Runx transcription factors, including Runx1, Runx2 and Runx3,[43] have been shown to coordinate various cellular processes, including cell proliferation, development, differentiation, and interactions.[44,45] Runx is widely expressed in various tissues, especially mesenchymal condensates[46] and has primarily been identified to regulate osteoblast phenotype.[47] In addition, previous studies have substantiated that Runx2 is a critical mechanistic link among mitosis, ribosomal biogenesis and cell fate,[48] and is involved in cancer metastasis,[49] vascular and valve calcification[26,50] and neurodegenerative diseases.[51] In the present study, immunoprecipitation coupled with mass spectrometry (IP-MS) assessment of NRVM lysates determined that Alox5 could directly target Runx2 and promoted the nuclear localization of Runx2. Our findings highlight the critical role of Runx2 in cardiomyocytes. Most recently, it has been suggested that liquid–liquid phase separation (LLPS) of transcription factors is essential for transcriptional activity and regulates multiple biological functions, including chromatin organization, mitophagy and nucleosome.[52–54] This study analyzed the characteristic LLPS of Runx2 in hypertrophic stress-treated cardiomyocytes. We found that Alox5 deletion exerted a strong antagonistic effect against the LLPS of Runx2, resulting in the transcriptional activation of Runx2 in NRVMs. Our finding filled this knowledge gap and demonstrated that LLPS of transcription factors was crucial for cardiac remodeling and HF.

Best known as a member of the ErbB family of tyrosine kinase receptors,[55] the epidermal growth factor receptor (EGFR) is a transmembrane glycoprotein present in multiple types of cells.[56] EGFR has been strongly identified as a therapeutic target for cancer and metastasis.[57,58] In addition, EGFR signaling has been generally reported to regulate cardiac regeneration,[59] cardiac hypertrophy[60] and fibrosis.[61] An increasing body of evidence suggests that mitogen-activated protein kinase (MAPK) is involved in cardiac hypertrophy[62] and ventricular remodeling.[63] In the present study, transcriptomic assessment determined that Alox5 deficiency downregulated EGFR and MAPK pathways to suppress cardiac remodeling and HF under chronic pressure overload conditions. More importantly, Alox5 markedly upregulated the transcriptional activity of Runx2, which could directly bind with the EGFR promoter and accelerate EGFR mRNA generation in cardiomyocytes, leading to cardiac remodeling.

Limitations

This study has several limitations. An increasing body of evidence suggests that several promising small molecular inhibitors targeting Alox5 served as crucial suppressor of inflammation, while whether some of these small molecular inhibitors could impede Runx2 signaling to attenuate ventricular remodeling is worth further validation. In addition, despite the limited effects of Alox5 have been interpreted in cells of myeloid origin, the cardiac resident macrophages are not ruled out. In LLPS formation of RUNX2, utilization of human

***Fig. 7*: Transcriptional repression domain is required for Runx2 phase separation and Knockdown of Runx2 abrogates Alox5 overexpression-mediated cardiomyocyte hypertrophy in vitro. a.** Domain structure of Runx2 truncations. **b.** Confocal microscopy images of NRVMs transfected with various Runx2 truncations as indicated under Veh and Ang II (100 nM, 24 h) conditions. **c.** Primary cardiomyocytes were infected with adenovirus overexpressing Alox5 (Ad-Alox5) or empty vector GFP (Ad-GFP) together with siRNA-Runx2 or siRNA-control, and then treated with Veh or Ang II (100 nM) for 24 h. Representative images of immunostaining targeting α-actinin of NRVMs (left) and quantification of myocyte surface area (right) (n = 3 independent experiments). **d.** qPCR analysis of Nppa mRNA expression in NRVMs (n = 3). One-way ANOVA with Tukey's post-hoc test. **e** and **f.** Representative immunoblotting analysis and quantification of the protein levels of Alox5, Runx2, p-P38, T-P38, p-ER1/2, T-ERK1/2, p-JNK, T-JNK, p-EGFR and T-EGFR (n = 4). β-Tubulin as an internal control. One-way ANOVA with Tukey's post-hoc test. **g.** Schematic representation of Alox5 and Runx2 in cardiomyocytes after hypertrophic stimuli. The results are shown as mean ± SEM. P values are indicated.

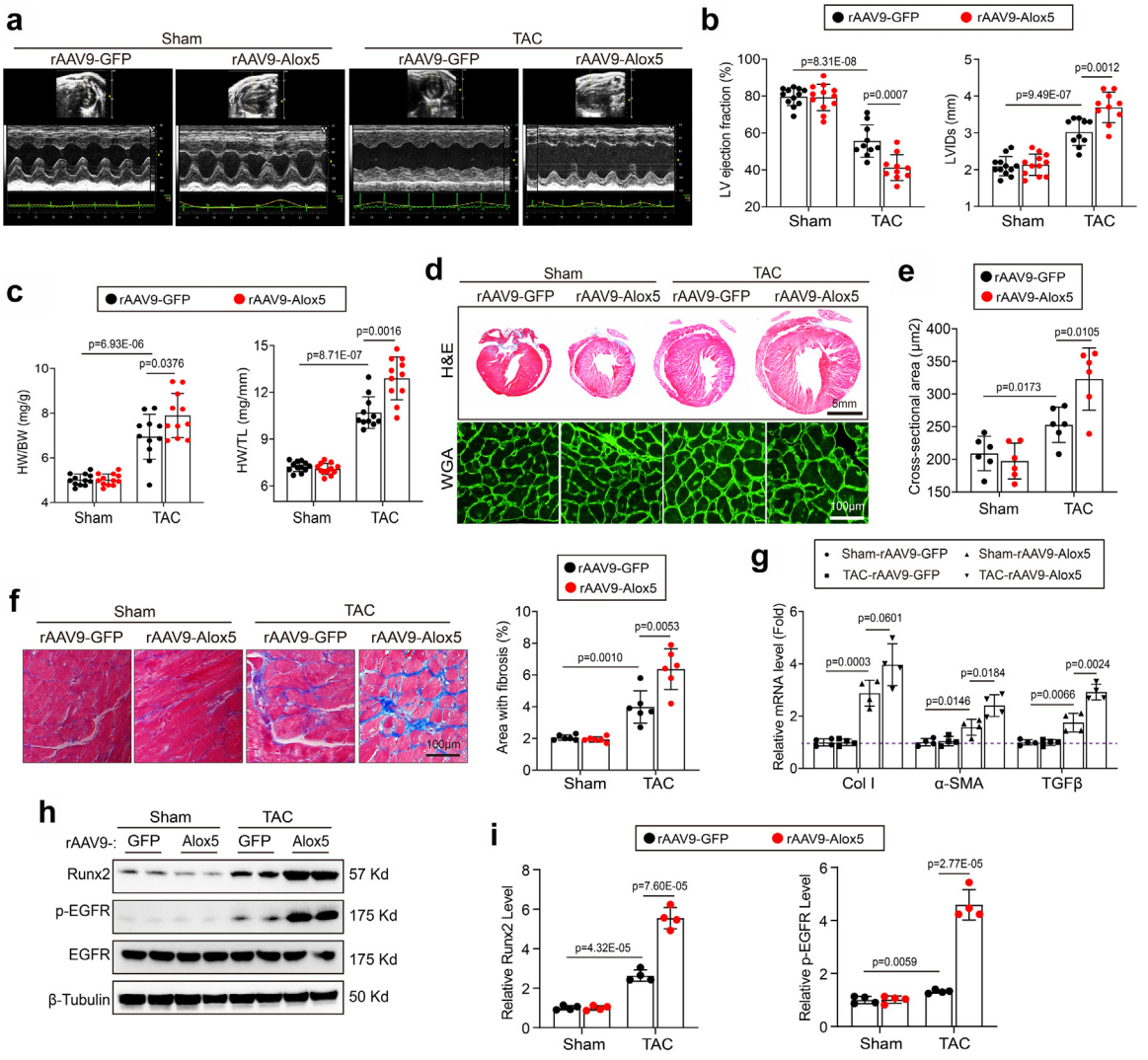

***Fig. 8:* Alox5 overexpression aggravates cardiac remodeling and dysfunction in mice.** C57BL/6J mice received rAAV9-GFP or rAAV9-cTnT-Alox5 were subjected to TAC for 6 weeks. **a** and **b.** Representative B- and M-mode echocardiographic imaging of heart, **b.** analysis of LVEF and LVIDs of hearts subjected to TAC surgery (n = 10–12). Two-way ANOVA with Tukey's post hoc test. **c.** Heart to body weight (HW/BW) and heart weight to tibia length (HW/TL) ratios (n = 10–12). Two-way ANOVA with Tukey's post hoc test. **d.** Representative H&E and WGA-stained sections (n = 6). **e.** Quantification of myocyte cross-sectional area (n = 6). Two-way ANOVA with Tukey's post hoc test. **f.** Representative cardiac Masson trichrome staining in heart tissues (left), and quantification of positive area with fibrosis (right) (n = 6). Two-way ANOVA with Tukey's post hoc test. **g.** qPCR quantification of collagen I, α-SMA and TGFβ mRNA in heart tissues (n = 4). Two-way ANOVA with Tukey's post hoc test. **h** and **i.** Representative immunoblotting analysis and quantification of the protein levels of Runx2, p-EGFR and EGFR (n = 4). Two-way ANOVA with Tukey's post hoc test. The results are shown as mean ± SEM. P values are indicated.

engineering cells maybe more meaningful. On the other hand, although we observed the hypertrophic phenotype through knock down Runx2 in Alox5 overexpression model, inhibiting LLPS of Runx2 or blockage of the interaction between Runx2 and Alox5 maybe more significance, which might be worth further investigation.

In conclusion, significant cardiac Alox5 expression was associated with cardiac structure remodeling and dysfunction. Genetic depletion of Alox5 attenuated pathological ventricular remodeling. Moreover, Alox5 expression in cardiomyocytes, not in bone marrow-derived macrophages, determined susceptibility to cardiac remodeling and HF. Also, cardiac-specifical Alox5 overexpression exaggerates TAC-induced cardiac remodeling. Mechanistically, we demonstrated that Alox5 could directly bind to Runx2 and promote nuclear localization of Runx2 in an enzymatic activity-independent manner, contributing to liquid–liquid

phase separation (LLPS) of Runx2 in the nucleus and activation of EGFR and MAPK pathways in cardiomyocytes. Overall, the present study identified Alox5 as the critical driving force of cardiac remodeling and HF and proposed Alox5 as a potential therapeutic target against cardiac structure remodeling and dysfunction.

Contributors

Qizhu Tang and Saiyang Xie designed research, Saiyang Xie and Chen Liu carried out experiments and Wei Deng analyzed data. Yun Xing and Man Xu carried out animal and mass spectrometry experiments. Min Zhang and Wenxi Fang assisted with immunoblot experiments. Shiqiang Liu and Xiaofeng Zeng oversaw flow cytometry experiments. Saiyang Xie and Shasha Wang co-wrote the paper. Qizhu Tang and Wei Deng prepared the proofread document. Qingqing Wu, Wenke Shi, Mengya Chen and Si Chen accessed and verified the underlying data. All authors read and approved the final version of the manuscript, and ensure it is the case.

Data sharing statement

All relevant data in the manuscript will be shared by the lead contact upon request.

Declaration of interests

The authors declared that the research was conducted in the absence of any commercial or financial relationships that could be construed as a potential conflict of interest.

Acknowledgments

The work of the authors is supported by grants from the National Natural Science Foundation of China (No: 81860080, 82170245 and 81700254); the National Key R&D Program of China (2018YFC1311300); the Key Project of the National Natural Science Foundation of China (No. 81530012); the Fundamental Research Funds for the Central Universities (2042018kf1032). The authors thank Frontier Science Center for Immunology and Metabolism, Medical Research Institution of Wuhan University for assistance with Rad Source RS2000Pro, Institute of Hydrobiology in Chinese Academy of Sciences for providing BD FACS Celesta.

Appendix A. Supplementary data

Supplementary data related to this article can be found at https://doi.org/10.1016/j.ebiom.2022.104359.

References

1 Cohn JN, Ferrari R, Sharpe N. Cardiac remodeling–concepts and clinical implications: a consensus paper from an international forum on cardiac remodeling. Behalf of an International Forum on Cardiac Remodeling. *J Am Coll Cardiol*. 2000;35:569–582.
2 Modica J, Di Mauro V, Barandalla-Sobrados M, et al. Nano-miR-133a replacement therapy blunts pressure overload-induced heart failure. *Circulation*. 2021;144:1973–1976.
3 Santos-Zas I, Lemarie J, Zlatanova I, et al. Cytotoxic CD8(+) T cells promote granzyme B-dependent adverse post-ischemic cardiac remodeling. *Nat Commun*. 2021;12:1483.
4 Shugg T, Hudmon A, Overholser BR. Neurohormonal regulation of IKs in heart failure: implications for ventricular arrhythmogenesis and sudden cardiac death. *J Am Heart Assoc*. 2020;9:e016900.
5 Suetomi T, Willeford A, Brand CS, et al. Inflammation and NLRP3 inflammasome activation initiated in response to pressure overload by Ca(2+)/calmodulin-dependent protein kinase ii delta signaling in cardiomyocytes are essential for adverse cardiac remodeling. *Circulation*. 2018;138:2530–2544.
6 Tajiri K, Guichard JB, Qi X, et al. An N-/L-type calcium channel blocker, cilnidipine, suppresses autonomic, electrical, and structural remodelling associated with atrial fibrillation. *Cardiovasc Res*. 2019;115:1975–1985.
7 Karam S, Margaria JP, Bourcier A, et al. Cardiac overexpression of PDE4B blunts beta-adrenergic response and maladaptive remodeling in heart failure. *Circulation*. 2020;142:161–174.
8 Pugliese NR, Masi S, Taddei S. The renin-angiotensin-aldosterone system: a crossroad from arterial hypertension to heart failure. *Heart Fail Rev*. 2020;25:31–42.
9 Skrzypczak-Jankun E, Jankun J, Al-Senaidy A. Human lipoxygenase: developments in its structure, function, relevance to diseases and challenges in drug development. *Curr Med Chem*. 2012;19:5122–5127.
10 Tomita K, Takashi Y, Ouchi Y, et al. Lipid peroxidation increases hydrogen peroxide permeability leading to cell death in cancer cell lines that lack mtDNA. *Cancer Sci*. 2019;110:2856–2866.
11 Zhang XJ, Liu X, Hu M, et al. Pharmacological inhibition of arachidonate 12-lipoxygenase ameliorates myocardial ischemia-reperfusion injury in multiple species. *Cell Metab*. 2021;33:2059–2075 e10.
12 Suzuki H, Kayama Y, Sakamoto M, et al. Arachidonate 12/15-lipoxygenase-induced inflammation and oxidative stress are involved in the development of diabetic cardiomyopathy. *Diabetes*. 2015;64:618–630.
13 Gilbert NC, Gerstmeier J, Schexnaydre EE, et al. Structural and mechanistic insights into 5-lipoxygenase inhibition by natural products. *Nat Chem Biol*. 2020;16:783–790.
14 Lai Q, Yuan G, Shen L, et al. Oxoeicosanoid receptor inhibition alleviates acute myocardial infarction through activation of BCAT1. *Basic Res Cardiol*. 2021;116:3.
15 Dufrusine B, Di Francesco A, Oddi S, et al. Iron-dependent trafficking of 5-lipoxygenase and impact on human macrophage activation. *Front Immunol*. 2019;10:1347.
16 Fischer J, Gresnigt MS, Werz O, et al. Candida albicans-induced leukotriene biosynthesis in neutrophils is restricted to the hyphal morphology. *FASEB J*. 2021;35:e21820.
17 Botan V, Dos Santos Borges TK, Rocha Alves EA, et al. Enhanced activation of eosinophils in peripheral blood and implications for eosinophilic esophagitis diagnosis. *J Gastroenterol Hepatol*. 2017;32:1318–1327.
18 Xie S, Qi X, Wu Q, et al. Inhibition of 5-lipoxygenase is associated with downregulation of the leukotriene B4 receptor 1/Interleukin-12p35 pathway and ameliorates sepsis-induced myocardial injury. *Free Radic Biol Med*. 2021;166:348–357.
19 Almeida SO, Ram RJ, Kinninger A, et al. Effect of 5-lipoxygenase inhibitor, VIA-2291 (atreleuton), on epicardial fat volume in patients with recent acute coronary syndrome. *J Cardiovasc Comput Tomogr*. 2020;14:343–348.
20 Gaztanaga J, Farkouh M, Rudd JH, et al. A phase 2 randomized, double-blind, placebo-controlled study of the effect of VIA-2291, a 5-lipoxygenase inhibitor, on vascular inflammation in patients after an acute coronary syndrome. *Atherosclerosis*. 2015;240:53–60.
21 Zhang W, Zhou Y, Bai B, et al. Consistency of left ventricular hypertrophy diagnosed by electrocardiography and echocardiography: the Northern Shanghai Study. *Clin Interv Aging*. 2019;14:549–556.
22 Wang HB, Yang J, Shuai W, et al. Deletion of microfibrillar-associated protein 4 attenuates left ventricular remodeling and dysfunction in heart failure. *J Am Heart Assoc*. 2020;9:e015307.
23 Acin-Perez R, Iborra S, Marti-Mateos Y, et al. Fgr kinase is required for proinflammatory macrophage activation during diet-induced obesity. *Nat Metab*. 2020;2:974–988.
24 Gerstmeier J, Newcomer ME, Dennhardt S, et al. 5-Lipoxygenase-activating protein rescues activity of 5-lipoxygenase mutations that delay nuclear membrane association and disrupt product formation. *FASEB J*. 2016;30:1892–1900.
25 Flamand N, Lefebvre J, Surette ME, et al. Arachidonic acid regulates the translocation of 5-lipoxygenase to the nuclear membranes in human neutrophils. *J Biol Chem*. 2006;281:129–136.
26 Eva Sikura K, Combi Z, Potor L, et al. Hydrogen sulfide inhibits aortic valve calcification in heart via regulating RUNX2 by NF-kappaB, a link between inflammation and mineralization. *J Adv Res*. 2021;27:165–176.
27 Ishii S, Noguchi M, Miyano M, et al. Mutagenesis studies on the amino acid residues involved in the iron-binding and the activity of

human 5-lipoxygenase. *Biochem Biophys Res Commun*. 1992;182:1482–1490.
28 Lu Y, Wu T, Gutman O, et al. Phase separation of TAZ compartmentalizes the transcription machinery to promote gene expression. *Nat Cell Biol*. 2020;22:453–464.
29 Chen D, Wang Z, Zhao YG, et al. Inositol polyphosphate multikinase inhibits liquid-liquid phase separation of TFEB to negatively regulate autophagy activity. *Dev Cell*. 2020;55:588–602.e7.
30 Boija A, Klein IA, Sabari BR, et al. Transcription factors activate genes through the phase-separation capacity of their activation domains. *Cell*. 2018;175:1842–1855.e16.
31 ter Maaten JM, Valente MA, Damman K, et al. Diuretic response in acute heart failure-pathophysiology, evaluation, and therapy. *Nat Rev Cardiol*. 2015;12:184–192.
32 Rurik JG, Tombacz I, Yadegari A, et al. CAR T cells produced in vivo to treat cardiac injury. *Science*. 2022;375:91–96.
33 Roos J, Grosch S, Werz O, et al. Regulation of tumorigenic Wnt signaling by cyclooxygenase-2, 5-lipoxygenase and their pharmacological inhibitors: a basis for novel drugs targeting cancer cells? *Pharmacol Ther*. 2016;157:43–64.
34 Lin Y, Cai Q, Chen Y, et al. CAFs shape myeloid-derived suppressor cells to promote stemness of intrahepatic cholangiocarcinoma through 5-lipoxygenase. *Hepatology*. 2022;75:28–42.
35 Taccone-Gallucci M, Manca-di-Villahermosa S, Battistini L, et al. N-3 PUFAs reduce oxidative stress in ESRD patients on maintenance HD by inhibiting 5-lipoxygenase activity. *Kidney Int*. 2006;69:1450–1454.
36 Stanke-Labesque F, Back M, Lefebvre B, et al. Increased urinary leukotriene E4 excretion in obstructive sleep apnea: effects of obesity and hypoxia. *J Allergy Clin Immunol*. 2009;124:364–370, 370.e1–2.
37 Shajari S, Laliena A, Heegsma J, et al. Melatonin suppresses activation of hepatic stellate cells through RORalpha-mediated inhibition of 5-lipoxygenase. *J Pineal Res*. 2015;59:391–401.
38 Demetz E, Schroll A, Auer K, et al. The arachidonic acid metabolome serves as a conserved regulator of cholesterol metabolism. *Cell Metab*. 2014;20:787–798.
39 Powell WS, Rokach J. The eosinophil chemoattractant 5-oxo-ETE and the OXE receptor. *Prog Lipid Res*. 2013;52:651–665.
40 Giannopoulos PF, Chu J, Sperow M, et al. Pharmacologic inhibition of 5-lipoxygenase improves memory, rescues synaptic dysfunction, and ameliorates tau pathology in a transgenic model of tauopathy. *Biol Psychiatry*. 2015;78:693–701.
41 Van Anh TT, Mostafa A, Rao Z, et al. From Vietnamese plants to a biflavonoid that relieves inflammation by triggering the lipid mediator class switch to resolution. *Acta Pharm Sin B*. 2021;11:1629–1647.
42 Tardif JC, L L'Allier P, Ibrahim R, et al. Treatment with 5-lipoxygenase inhibitor VIA-2291 (atreleuton) in patients with recent acute coronary syndrome. *Circ Cardiovasc Imaging*. 2010;3:298–307.
43 de Bruijn M, Dzierzak E. Runx transcription factors in the development and function of the definitive hematopoietic system. *Blood*. 2017;129:2061–2069.
44 Mevel R, Draper JE, Lie ALM, et al. RUNX transcription factors: orchestrators of development. *Development*. 2019;146:dev148296.
45 McCarroll CS, He W, Foote K, et al. Runx1 deficiency protects against adverse cardiac remodeling after myocardial infarction. *Circulation*. 2018;137:57–70.
46 Zhou G, Zheng Q, Engin F, et al. Dominance of SOX9 function over RUNX2 during skeletogenesis. *Proc Natl Acad Sci U S A*. 2006;103:19004–19009.
47 Satpathy AT, Briseno CG, Cai X, et al. Runx1 and Cbfbeta regulate the development of Flt3+ dendritic cell progenitors and restrict myeloproliferative disorder. *Blood*. 2014;123:2968–2977.
48 Young DW, Hassan MQ, Pratap J, et al. Mitotic occupancy and lineage-specific transcriptional control of rRNA genes by Runx2. *Nature*. 2007;445:442–446.
49 Sancisi V, Manzotti G, Gugnoni M, et al. RUNX2 expression in thyroid and breast cancer requires the cooperation of three non-redundant enhancers under the control of BRD4 and c-JUN. *Nucleic Acids Res*. 2017;45:11249–11267.
50 Wang C, Xu W, An J, et al. Poly(ADP-ribose) polymerase 1 accelerates vascular calcification by upregulating Runx2. *Nat Commun*. 2019;10:1203.
51 Chen JA, Chen Z, Won H, et al. Joint genome-wide association study of progressive supranuclear palsy identifies novel susceptibility loci and genetic correlation to neurodegenerative diseases. *Mol Neurodegener*. 2018;13:41.
52 Ahn JH, Davis ES, Daugird TA, et al. Phase separation drives aberrant chromatin looping and cancer development. *Nature*. 2021;595:591–595.
53 Gibson BA, Doolittle LK, Schneider MWG, et al. Organization of chromatin by intrinsic and regulated phase separation. *Cell*. 2019;179:470–484 e21.
54 Fang X, Wang L, Ishikawa R, et al. Arabidopsis FLL2 promotes liquid-liquid phase separation of polyadenylation complexes. *Nature*. 2019;569:265–269.
55 Schlessinger J. Cell signaling by receptor tyrosine kinases. *Cell*. 2000;103:211–225.
56 Yarden Y, Shilo BZ. SnapShot: EGFR signaling pathway. *Cell*. 2007;131:1018.
57 Chong CR, Janne PA. The quest to overcome resistance to EGFR-targeted therapies in cancer. *Nat Med*. 2013;19:1389–1400.
58 Zhong C, Yang J, Lu Y, et al. Achyranthes bidentata polysaccharide can safely prevent NSCLC metastasis via targeting EGFR and EMT. *Signal Transduct Target Ther*. 2020;5:178.
59 Aharonov A, Shakked A, Umansky KB, et al. ERBB2 drives YAP activation and EMT-like processes during cardiac regeneration. *Nat Cell Biol*. 2020;22:1346–1356.
60 Bi HL, Zhang XL, Zhang YL, et al. The deubiquitinase UCHL1 regulates cardiac hypertrophy by stabilizing epidermal growth factor receptor. *Sci Adv*. 2020;6:eaax4826.
61 Liu L, Jin X, Hu CF, et al. Amphiregulin enhances cardiac fibrosis and aggravates cardiac dysfunction in mice with experimental myocardial infarction partly through activating EGFR-dependent pathway. *Basic Res Cardiol*. 2018;113:12.
62 Lin HB, Naito K, Oh Y, et al. Innate immune Nod1/RIP2 signaling is essential for cardiac hypertrophy but requires mitochondrial antiviral signaling protein for signal transductions and energy balance. *Circulation*. 2020;142:2240–2258.
63 Liu R, van Berlo JH, York AJ, et al. DUSP8 regulates cardiac ventricular remodeling by altering ERK1/2 signaling. *Circ Res*. 2016;119:249–260.